AMERICAN UNIVERSITY OF BEIRUT

RENEWABLE ELECTRICAL ENERGY IN THE MEDITERRANEAN MENA: WAVE WIND AND SOLAR POTENTIAL

by
ANWAR GHASSAN AL SHAMI

A thesis
submitted in partial fulfillment of the requirements
for the degree of Master of Engineering
to the Department of Civil and Environmental Engineering
of the Faculty of Engineering and Architecture
at the American University of Beirut

Beirut, Lebanon
June 2016

AMERICAN UNIVERSITY OF BEIRUT

RENEWABLE ELECTRICAL ENERGY IN THE MEDITERRANEAN MENA: WAVE WIND AND SOLAR POTENTIAL

by

ANWAR GHASSAN AL SHAMI

Approved by:

Dr. Majdi Abou Najm, Assistant Professor Department of Civil and Environmental Engineering	Advisor
Dr. Mutasem Fadel, Professor Department of Civil and Environmental Engineering	Member of Committee
Dr. George Saad, Assistant Professor Department of Civil and Environmental Engineering	Member of Committee
Dr. Matthias Liermann, Assistant Professor Department of Mechanical Engineering	Member of Committee

Date of thesis defense: June 2016

AMERICAN UNIVERSITY OF BEIRUT

THESIS, DISSERTATION, PROJECT RELEASE FORM

Student Name: _____
Last First Middle

◯ Master's Thesis ◯ Master's Project ◯ Doctoral Dissertation

☐ I authorize the American University of Beirut to: (a) reproduce hard or electronic copies of my thesis, dissertation, or project; (b) include such copies in the archives and digital repositories of the University; and (c) make freely available such copies to third parties for research or educational purposes.

☐ I authorize the American University of Beirut, **three years after the date of submitting my thesis, dissertation, or project,** to: (a) reproduce hard or electronic copies of it; (b) include such copies in the archives and digital repositories of the University; and (c) make freely available such copies to third parties for research or educational purposes.

_____

Signature Date

ACKNOWLEDGMENTS

My recognition and gratitude are addressed to my friends and family for their invaluable support. Special thanks are for the members of my committee for their guidance and assistance.

AN ABSTRACT OF THE THESIS OF

Anwar Ghassan Al Shami for Master of Engineering
Major: Environmental and Water Resources Engineering

Title: Renewable Electrical Energy in the Mediterranean MENA: Wave, Wind and Solar Potentials

This study examines the environmental and economic implications of renewable energy (RE) deployment (wave, wind, solar, hydro) in the energy sector within the Middle Eastern and North Africa (MENA) countries falling on the rim of the Mediterranean. LEAP long term simulations of green-house gases (GHG) emissions were used under several scenarios at the country scale. MIKE21 SW simulations were used to provide input for LEAP regarding wave energy while inputs for wind, solar and hydro were obtained from the literature. Results showed that increased RE penetration in power generation in the study area is justified by the multitude of social benefits associated with RE including GHG emissions reductions, green jobs, sustainable energy, and energy security. While the initial investment in RE is relatively high, it is expected to decline with technology advances and economies of scale which will further facilitate and catalyze the shift to RE at the local and regional scales. Results showed that investment in wave energy is still associated with high costs that would prohibit its inclusion in an RE *penetration* energy due to the relatively low power density of the Mediterranean Sea and the developing nature of the technology.

CONTENTS

ACKNOWLEDGEMENTS v
ABSTRACT vi
LIST OF ILLUSTRATIONS ix
LIST OF TABLES x

Chapter

I. INTRODUCTION 1

II. MATERIALS AND METHODS 4

A. Study area 4

B. Data collection 4

1. MIKE21 SW 4
2. LEAP 7

C. Model descriptions and simulation scenarios 9

1. MIKE 21 SW 10
2. LEAP 17
3. Financial accounts analysis 19

III. RESULTS AND DISCUSSION 20

A. Wave resource 20

1. Validation 20
2. Simulation Output 20

B. RE Penetration 25

C. Economic implications 29

IV. CONCLUSION 33

Appendix

I. BRIEF OVERVIEW OF SPECTRAL WAVE THEORY 34
II. ANALYTICAL APPROXIMATION TO WAVE POWER..... 37
III. MIKE21SW DATA PROCESSING AND MODEL SETUP... 39
A. Mesh Generation 39
1. Coastline data 39
2. Bathymetry data 40
B. Forcing data 40
1. DFS2 precursor format 41
2. Script structure 43
C. Model setup 48
IV. ELECTRICAL ENERGY CONSUMPTION PER CAPITA ... 73

REFERENCES 75

ILLUSTRATIONS

Figure

1 Recent wave power studies conducted using third generation spectral wave models 2

2 Map of study area 5

3 15 year 6 hourly wind speeds averages by month in m/s 8

4 Electric power consumption (kWh per capita) 9

5 East Mediterranean sea computational mesh 14

6 Mediterranean Sea computational mesh 15

7 The Pelamis WEC (http://www.power-technology.com/projects/pelamis/) 16

8 Ayat 2013 study results (left), MIKE21 SW model results (right) 22

9 Mean wave power (in KW/m) for the 15 year dataset 23

10 Variation of wave power over frontage line 24

11 Energy sector GHG emissions in million tons of carbon dioxide equivalents (MtCO2e) for each scenario 26

12 Percent reduction in GHG emissions for the mitigation scenarios 27

13 GHG savings in MtCO2e of each scenario wrt baseline scenario 27

14 Estimated electricity generation costs in billions of USD (reference year 2010, discount rate 5%) 29

15 Percent change in investment for RE deployment scenarios with respect to the baseline scenario (Bn 2010 USD, i=0.05) 30

TABLES

Table

1 ECMWF parameter description 6

2 Simulation scenarios 18

3 Levelized cost of electricity generation per energy source in USD/MWh in 2010 dollars 19

4 Change in investment for mitigation scenarios wrt baseline scenarios 31

5 Mitigated GHG emissions under the RE penetration scenarios 32

CHAPTER I

INTRODUCTION

One of the main causers of global CO_2 and other greenhouse gases (GHG) emissions is the use of fossil fuels as the world's most substantial energy source [IEA, 2014]. Renewable energy (RE) sources are increasingly used to limit shortcomings of fossil fuel consumption. Several studies simulated the benefits associated with different RE penetration scenarios including GHG emissions reduction [Chedid et al., 2001, Cai et al., 2007, Tsoutsos et al., 2008, McPherson and Karney, 2014a, Blumsack and Xu, 2011, Føyn et al., 2011, Connolly et al., 2010a]. Such simulations require energy input and output analysis tools such as LEAP or PLAN [McPherson and Karney, 2014b, Connolly et al., 2010b].

Besides wind, solar and hydroelectric power, wave power is one of the emerging RE resources. The global wave power potential is estimated to be in the order of 10^{13}W [Panicker, 1976], a value comparable to the world's current power consumption [IEA, 2014]. The amount of wave energy varies widely with geographical location, with Australia and New Zealand having the world's highest power extraction potential [Arinaga and Cheung, 2012].

Over the course of more than two centuries, several devices were proposed for making use of wave power [Stahl, 1892, Leishman et al., 1976, Shaw, 1982, Brooke, 2003]. The potential power output of such devices is governed by the existing wave climate. Wave climate analysis follows from 3rd generation spectral wave modeling (MIKE 21 SW, SWAN, WAM, WAVEWATCH III) forced by wind data to hindcast the wave parameters over the period and area of study. Several wave power potential studies have

been made using third generation spectral wave models, and a summary of some of the more recent is mapped in Figure 1. Iglesias and Carballo investigated the wave power potential around the coast of Spain using WAM and SWAN model simulations [Iglesias et al., 2009, Iglesias and Carballo, 2009, Iglesias and Carballo, 2010a, Iglesias and Carballo, 2010b, Iglesias and Carballo, 2010c]. Hughes and Heap [2010] used AusWam to study the power potential around Australia. Also using SWAN simulations, Kim et al.[2011] investigated the power potential of the Korean peninsula. Henfridsson et al. [2007] investigated the area of the Baltic Sea and the Danish part of the North Sea for its power potential using MIKE 21 SW model simulations. Also using MIKE 21 SW, Ayat

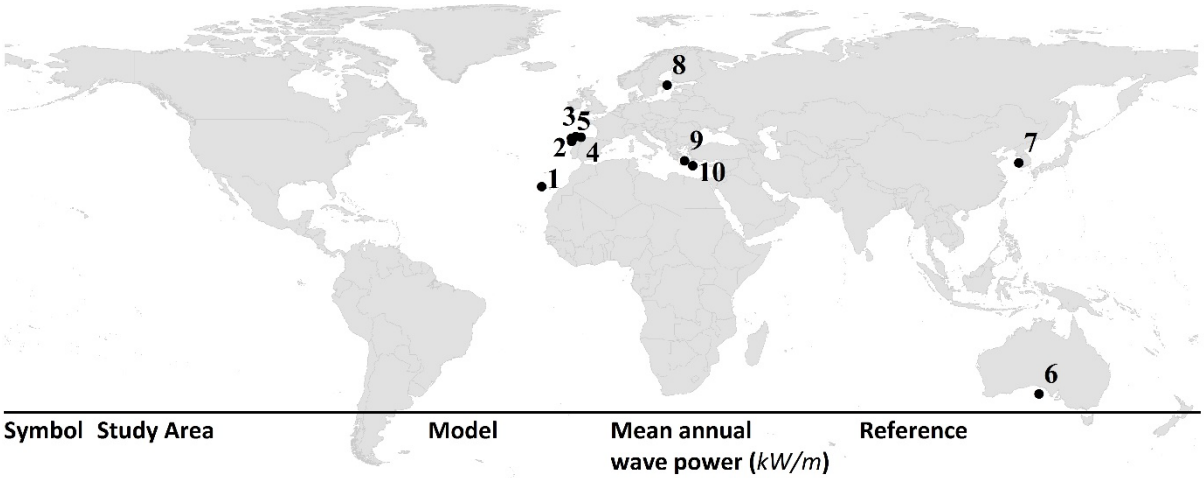

Symbol	Study Area	Model	Mean annual wave power (*kW/m*)	Reference
1	La Palma (Spain)	WAM	25	[Iglesias and Carballo, 2010c]
2	Death Coast (Spain)	WAM / SWAN	50	[Iglesias and Carballo, 2009]
3	Esteca de Bares (Spain)	SWAN	40	[Iglesias and Carballo, 2010b]
4	Asturias (Spain)	SWAN	30	[Iglesias and Carballo, 2010a]
5	Galicia (Spain)	WAM /SWAN	14.7	[Iglesias et al., 2009]
6	Australian shelf	AusWam	25-35	[Hughes and Heap, 2010]
7	Korea	SWAN	4-11	[Kim et al., 2011]
8	Baltic Sea	MIKE21SW	5	[Henfridsson et al., 2007]
9	Eastern Med. & Aegean seas	MIKE21SW	5	[Ayat, 2013]
10	Med.: Levantine Basin	WAM	2.5 (in coastal areas)	[Zodiatis et al., 2014]

[2013] made an assessment of the wave power potential of the Eastern

Figure 1 Recent wave power studies conducted using third generation spectral wave models

Mediterranean and Aegean Seas by using data for the years 1994-2009. Zodiatis et al. [2014], using WAM investigated the wave energy potential in the Eastern Mediterranean Levantine Basin. Up to this point there has been no study that hindcasts the wave power characteristics of the entire Mediterranean sea.

This study assesses the existing wave resource within the Middle Eastern and North Africa (MENA) countries falling on the rim of the Mediterranean sea using MIKE21 SW simulations, and examines the environmental and economic implications of RE (wave, wind, solar, hydro) deployment in the energy sector using long term simulations of GHG emissions under several scenarios on a country by country basis using LEAP.

CHAPTER II

MATERIALS AND METHODS

A. Study area

The study area includes the MENA countries that fall on the rim of the Mediterranean Sea (Algeria, Egypt, Israel, Lebanon, Libya, Morocco, Palestine, Syria, Tunisia and Turkey), a geopolitically diverse region that spans around 6.7 million square kilometers hosting about 290 million people (5% of the world total) living in a multitude of income statuses (Figure 2) [WorldBank, 2010].

B. Data collection

Data used in this study falls into two categories: weather and mesh building data used for wave modeling with MIKE21 SW; and scenario building data synthesized to be used with the Long Range Energy Alternatives Planning (LEAP) software.

1. MIKE21 SW

For the sake of wave modelling, the main source of weather data was the European Center for Medium range Weather Forecasts (ECMWF[#]). The ECMWF is an intergovernmental organization established in 1975 sustained by 34 states that aims to produce and archive numerical forecasts on the global level [Simmons et al., 2007]. The fields relevant for this study were acquired in binary format for the entire study area at a spatial resolution of $0.1° \times 0.1°$ and temporal resolution of 6 hours for a 15 years period (1994 to 2009). Parameter characteristics are summarized in Table 1.

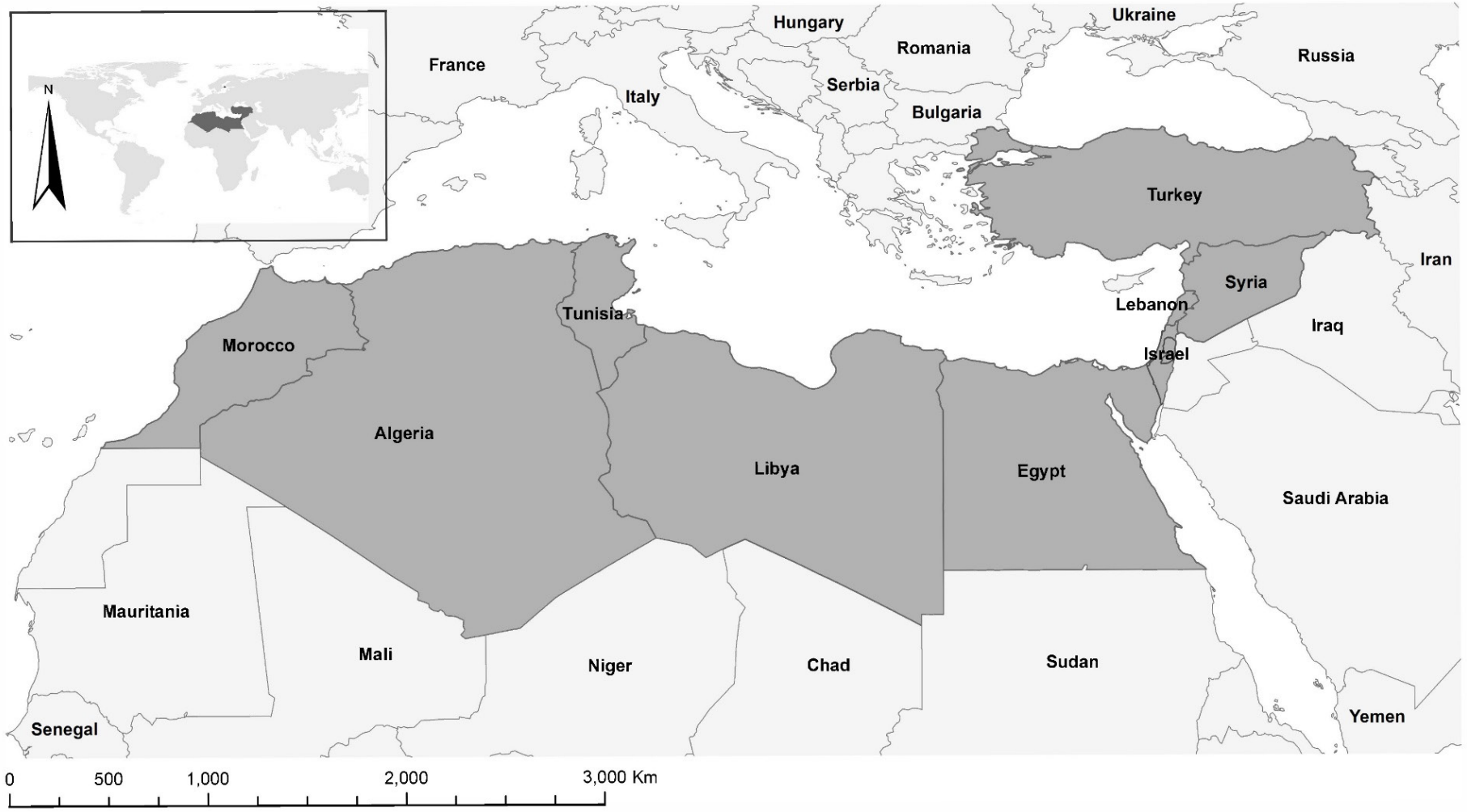

Figure 2 Map of study area

ECMWF parameters 165 and 166 that represent the U and V components of wind speed 10 meters above the surface were the inputs into third generation spectral wave modelling software MIKE21 SW as forcing data. Also required for wave modelling, the bathymetry and shorelines were obtained from the general bathymetric chart of the oceans (GEBCO - http://www.gebco. net/data_and_products/gridded_bathymetry_data/) and from the Global Self-consistent Hierarchal High-resolution Geography (GSHHG - https://www.soest.hawaii.edu/pwessel/ gshhg/) Database. Figure 3, generated from the data described in Table 1 using FERRET analysis system (package available at http://www.ferret.noaa.gov) shows the monthly averages of available wind data.

Table 1 ECMWF parameter description

Parameter	10m Wind speed- x direction[a]	10m Wind speed- y direction[b]
Unit	m/s	
Source	European center for medium range weather forecasts - ECMWF	
Time coordinates	01/01/1994 00:00 to 31/12/2010 00:00 time step: 6 hours	
Grid coordinates	points: 130 000 (250x520) lon: 21 to 46 by 0.1 degrees_east lat: -7 to 45 by 0.1 degrees_north	

[a] parameter 165 in the ECMWF interim reanalysis database;
[b] parameter 166 in the ECMWF interim reanalysis database

2. LEAP

RE penetration scenarios simulated in LEAP were obtained from El Fadel et al. [2013] based on secondary sources including country profiles, communication reports, assessment studies, databases and other sources. Electrical energy consumption per capita was obtained from the World Bank [2010] for each country from the year 1971 to 2012 in order for LEAP to extrapolate the electrical energy consumption trend for its modeled years. Values for the years 2002 through 2012 are shown in Figure 4. The full dataset is located in Appendix 4.

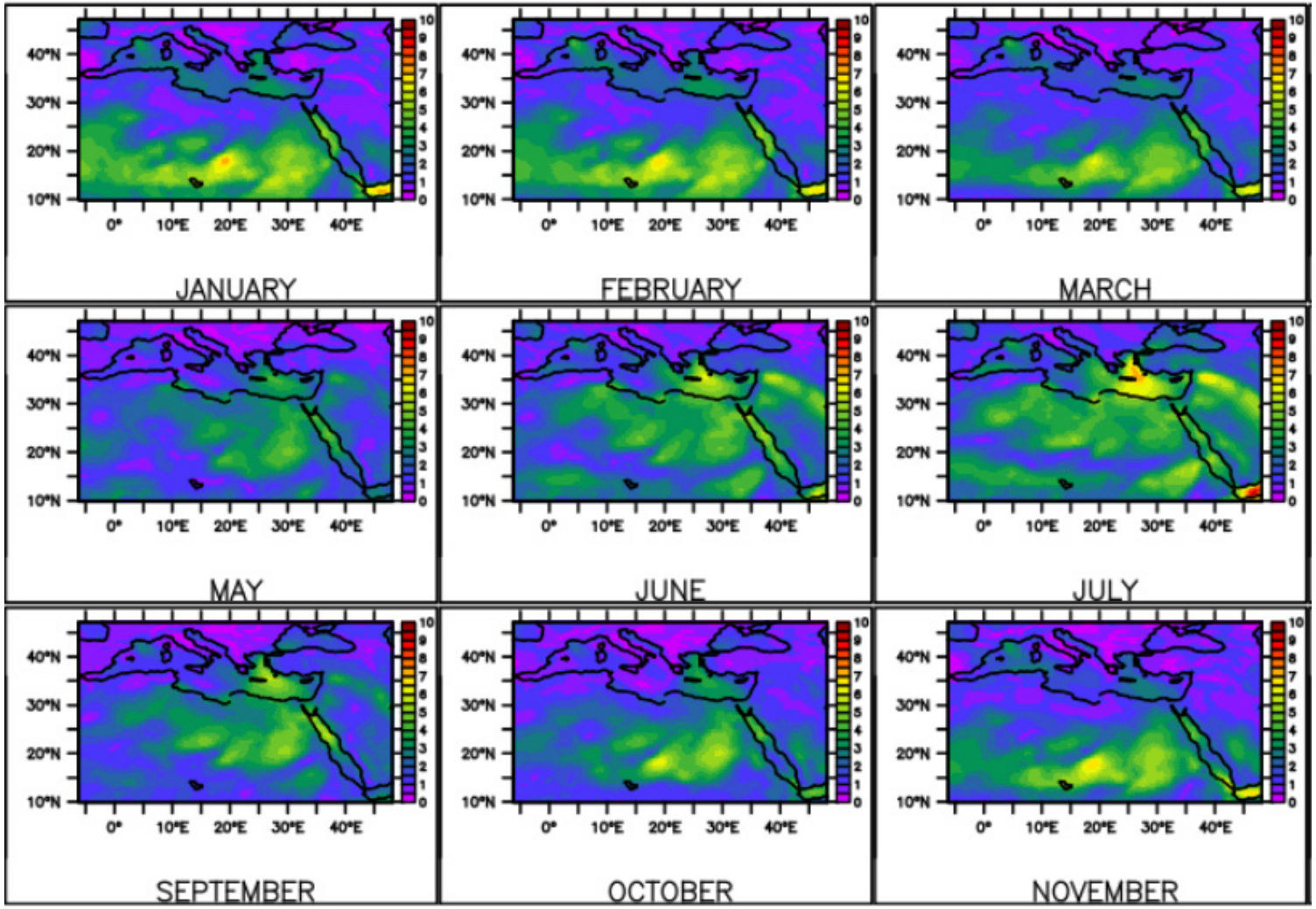

Figure 3 15 year 6 hourly wind speeds averages by month in m/s

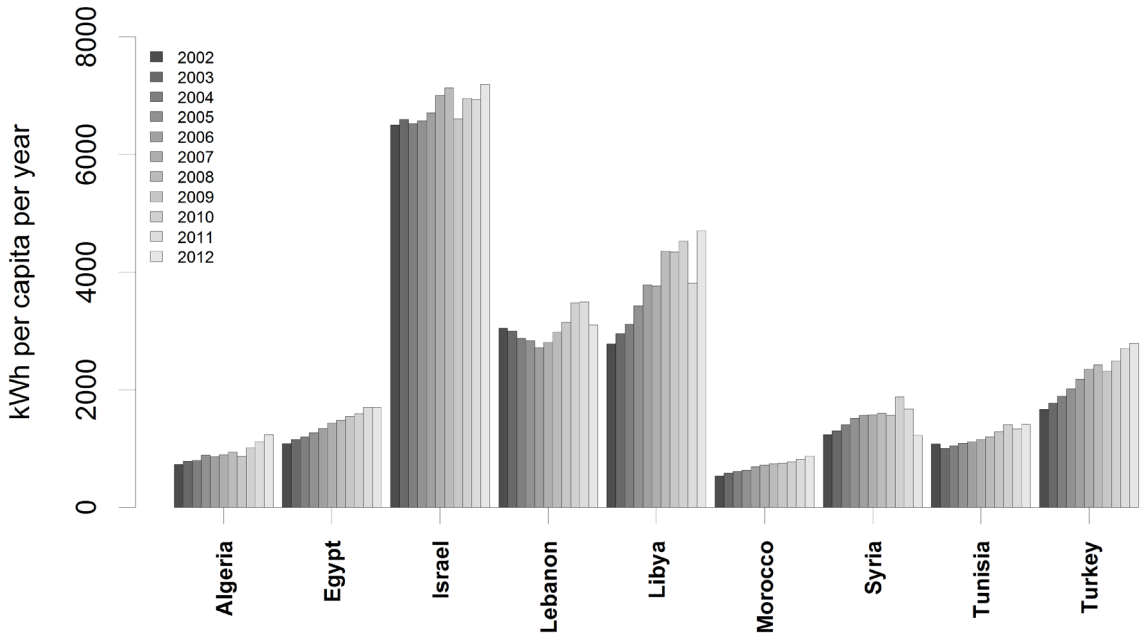

Figure 4 Electric power consumption (kWh per capita)

C. Model descriptions and simulation scenarios

When available, inputs to LEAP were obtained from the literature which provided the necessary information for wind, solar, and hydro (RE) as well as for oil, natural gas, and coal (conventional sources). Inputs relevant to wave energy were not completely available and thus were supplied from the outputs of MIKE 21 SW simulations for the Mediterranean sea. The following sections briefly explain the method used for MIKE 21 SW simulations as well as the utilization of LEAP to conduct the environmental and financial assessment.

1. LEAP

LEAP is an energy policy analysis tool developed by the Stockholm Environment Institute [SEI, 2016]. It was used to simulate several scenarios of RE penetration in the energy sector (electrical energy production) yielding results on country level GHG reduction and cost for each scenario.

The model was run for the period spanning between 2000 and 2040. Three mitigation scenarios with policy changes starting in year 2010 were compared to a baseline scenario assuming no changes in RE shares. Those four scenarios will be referred to as *Reference* (*Baseline*), *Policy, Revolution* and *RevolutionW* (Table 2). The *Reference* (*Baseline*), *Policy* and *Revolution* scenarios were adopted from [El Fadel et al., 2013] using the same energy mixes and sources (Oil, Solar, Hydroelectric power, Natural gas, Wind and Coal) with the *Baseline* scenario assuming status quo in RE penetration; the *Policy* scenario illustrating the expected reduction in GHG emissions given the respective countries' set targets; and the *Revolution* scenario illustrating the expected GHG emissions reduction assuming a flat rate of 66% in RE shares. The *RevolutionW* scenario is similar to the *Revolution* scenario while allowing for Wave energy extraction technology penetration with WEC shares in the energy mix obtained from the results of the MIKE21 SW model.

Table 2 Simulation scenarios

Country	Reference Scenario							Policy Scenario						
	Oil	Solar	Hydro	Nat.gas	Wind	Coal	Wave	Oil	Solar	Hydro	Nat.gas	Wind	Coal	Wave
Algeria	36	0	2	60	0	2	0	27	16	2	51	4	0	0
Egypt	16	0	11	73	0	0	0	11	16	11	58	4	0	0
Israel	11.8	0.15	0	18	0.05	70	0	0	18	0	70	12	0	0
Lebanon	88.08	0.02	11.9	0	0	0	0	0	3	12	80	5	0	0
Libya	59	0	0	41	0	0	0	44	20	0	36	0	0	0
Morocco	33	0	24	7	2	34	0	20	16	24	17	2	21	0
Syria	50	0	22	19	0	9	0	13	10	20	47	10	0	0
Tunisia	42.4	13.6	0	44	0	0	0	38.1	15	0	43.9	3	0	0
Turkey	8	6	20	38	5	23	0	3	10	26	36	5	20	0

Country	Revolution scenario							RevolutionW scenario						
	Oil	Solar	Hydro	Nat.gas	Wind	Coal	Wave	Oil	Solar	Hydro	Nat.gas	Wind	Coal	Wave
Algeria	10	48	6	24	12	0	0	10	43.2	6	24	12	0	4.8
Egypt	0	40	9	34	17	0	0	0	37.33	9	34	17	0	2.67
Israel	0	33	0	34	33	0	0	0	32.55	0	34	33	0	0.45
Lebanon	0	30	25	34	11	0	0	0	26.5	25	34	11	0	3.5
Libya	15	36	0	19	10	0	0	15	22.5	0	19	10	0	13.5
Morocco	15	24	32	12	10	7	0	15	20.7	32	12	10	7	3.3
Syria	10	18	30	24	18	0	0	10	17.52	30	24	18	0	0.48
Tunisia	15	49	0	19	17	0	0	15	38.3	0	19	17	0	10.7
Turkey	0	20	36	22	10	12	0	0	18.11	36	22	10	12	1.89

2. MIKE 21 SW

MIKE21 SpectralWave (SW) 3rd generation spectral wave model was used to estimate the wave resource potential by solving for the wave fields required to calculate wave power based on the spectral wave theory. Spectral wave theory's origins are in "description of noise" by Tukey and Hamming in their book "Measuring noise color 1" published in 1948 [Brillinger, 2002] and first applied to ocean waves by Barber and Ursell in 1948 and Deacon in 1949. MIKE21 SW was used to simulate the growth, decay and transformation of wind generated waves in the Mediterranean Sea. It accounts for wind wave generation, non-linear quadruplet wave-wave interaction, dissipation due to white-capping, bottom friction and depth-induced wave breaking, refraction and shoaling [DHI, 2012]. A brief overview of spectral wave theory is available in Appendix 1. An analytical approximation of average wave power per unit length of wave crest is discussed in Appendix 2 and is defined by:

$$\overline{P} = \frac{1}{4}\frac{L}{T}\left[1 + \frac{(\frac{4\pi d}{L})}{\sinh\left(\frac{4\pi d}{L}\right)}\right]\rho g H^2 \quad (1)$$

Where L is the wave length in meters, T is the peak wave period in seconds, H is the significant wave height in meters, and d, ρ, g are water depth, water density and gravitational acceleration respectively.

MIKE21 SW discretizes the conservation of wave action (Equation 4) in spectral and geographical space using an unstructured, cell centered finite volume method. It bases the time integration on a fractional step approach with an explicit method used to solve the propagation of wave action. To counteract restrictions on the time step caused by the use of such an explicit method, a multi-sequence explicit integration scheme is applied [Sorensen et al., 2004] [DHI, 2012].

MIKE 21 SW solves for wave action density spectrum which contains all the information necessary to fully describe gravity waves. Wave action density spectra $N(\sigma, \theta)$ are used in spectral wave models instead of wave energy spectra $E(\sigma, \theta)$ since, contrary to action density, energy density is not conserved during propagation in the presence of ambient current [Longuet-Higgins and Stewart, 1960]. The wave action density spectrum varies in space and time and is a function of two phase parameters. The two wave phase parameters are wave direction θ and the relative angular frequency σ. Action density and energy density are closely related as shown in Equation 2. Furthermore, the relative radian frequency is related to the absolute radian frequency $\omega = 2\pi f$ by the linear dispersion equation shown in Equation 3 [US Army Corps Of Engineers, 2002].

$$N(\sigma, \theta) = \frac{E(\sigma, \theta)}{\sigma} \tag{2}$$

$$\sigma = \sqrt{gk \tanh(kd)} = \omega - k.\vec{U} \tag{3}$$

Where $\sigma = 2\pi f_r$ is the relative radian frequency, g is the gravitational acceleration, d is the depth, $k = 2\pi/\lambda$ is the wave number and $\vec{U}$ is the current velocity vector.

The conservation equation for wave action in Cartesian coordinates is shown in Equation 4. MIKE 21 SW solves this equation for the wave parameters at all mesh points.

$$\frac{\partial N}{\partial t} + \nabla \cdot (\overline{v} N) = \frac{S}{\sigma} \tag{4}$$

Where S is the source/sink term for all physical processes that generate, dissipate or redistribute wave energy (detailed in Equation 8), ∇ is the four dimensional differential operator in $x = (x, y)$, σ, θ space. $v = (c_x, c_y, c_\sigma, c_\theta)$ is the propagation velocity in x, σ, θ space. The propagation speeds c_x, c_y, c_σ and c_θ are represented in Equations 5 to 8 [DHI, 2012].

$$(c_x, c_y) = \overrightarrow{c_g} + \vec{U} \tag{5}$$

$$c_g = \frac{\partial \sigma}{\partial k} = \frac{1}{2} \left(1 + \frac{2kd}{\sinh(2kd)}\right) \frac{\sigma}{h} \tag{6}$$

$$c_\sigma = \frac{d\sigma}{dt} = \frac{\partial \sigma}{\partial d} \left[\frac{\partial d}{\partial t} + \vec{U} \cdot \nabla_{\vec{x}} d\right] - c_g \vec{k} \frac{\partial \vec{U}}{\partial s} \tag{7}$$

$$c_\theta = \frac{d\sigma}{dt} = \frac{1}{k} \left[\frac{\partial \sigma}{\partial d} \frac{\partial d}{\partial m} + \vec{k} \cdot \frac{\partial \vec{U}}{\partial m}\right] \tag{8}$$

Where ∇_x in Equation 7 is the differential operator in the *x* space; *s* in Equation 7 is the space coordinate along *θ;* and *m* (Equation 8) is the perpendicular to *s*.

S (Equation 9) in the action balance equation (Equation 4) represents a sum of source/sink functions for several physical phenomena accounted for in MIKE 21 SW [DHI, 2012].

$$S = S_{in} + S_{nl} + S_{ds} + S_{bot} + S_{surf} \tag{9}$$

Here, S_{in} accounts for wave generation by wind, S_{nl} accounts for wave energy transfer due to non-linear quadruplet wave-wave interaction, S_{ds} is the dissipation of wave energy due to white capping, S_{bot} is the dissipation due to bottom friction and S_{surf} is dissipation due to depth induced breaking [DHI, 2012]. The flux of energy per unit crest width, widely known as wave power P is defined in equation 10 below. In this study, wave power is calculated using equation 10. The data processing required to run MIKE21SW and the exact model setup is discussed in detail in Appendix 3.

$$P = \rho g \int_0^{2\pi} \int_0^{\infty} c_g(f, \theta) E(f, \theta)\, df\, d\theta \tag{10}$$

In order to investigate the wave power extraction feasibility within the study area, the Ayat [2013] results were used to validate this study's model for the Eastern

Mediterranean and Aegean Sea and then reapplied to the entire Mediterranean Sea for use in assessing the available wave resource.

Mike 21 SW was run for the Eastern Mediterranean Sea mesh shown in Figure 5 in order to validate congruence with the Ayat results. The mesh area covers the Mediterranean Sea from 31^oN to 41^oN and 22^oW to 36^oE and is composed of 13,651 elements and 8,139 nodes. Ayat [2013] conducted an assessment of the wave power potential of the Eastern Mediterranean and the Aegean Seas by using data for the years 1994-2009. Using MIKE21 SpectralWave 3rd generation spectral wave model, Ayat obtained the wave fields by using data from the ECMWF interim reanalysis database [Simmons et al., 2007].

Once validated, and using the same parameters, the model was run for a mesh covering the entire Mediterranean sea (Figure 6) in order to assess the wave power potential of the study area. The Mediterranean Sea mesh has 23,995 elements and 14,585 nodes.

The Pelamis (Figure 7) was adopted as a benchmark for wave energy conversion technologies in the study. It is an attenuator type Wave Energy Converter (WEC) and was

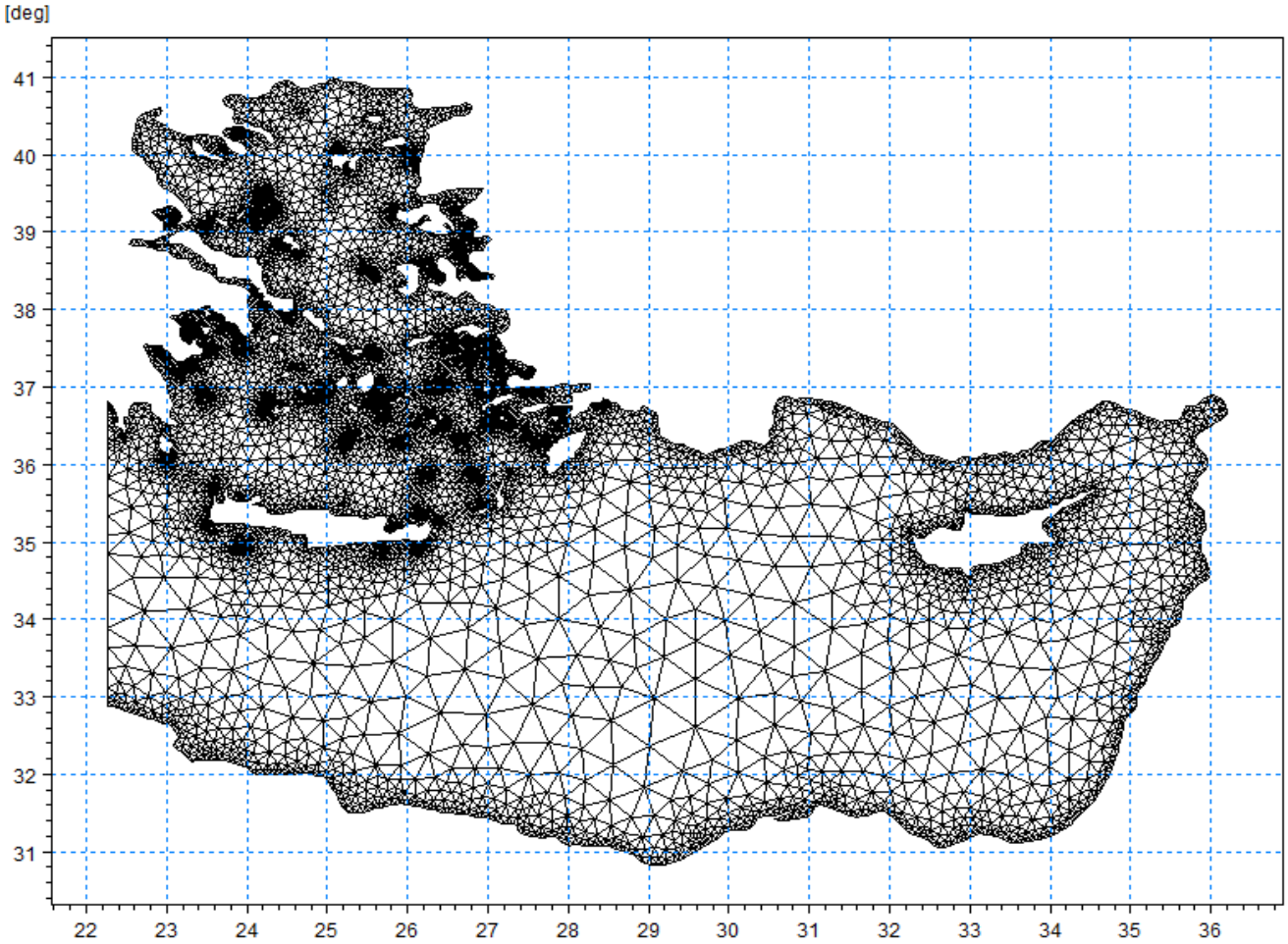

Figure 1 East Mediterranean sea computational mesh

the world's first offshore grid connected WEC in 2004 in the UK [Norris and Droniou, 2007].

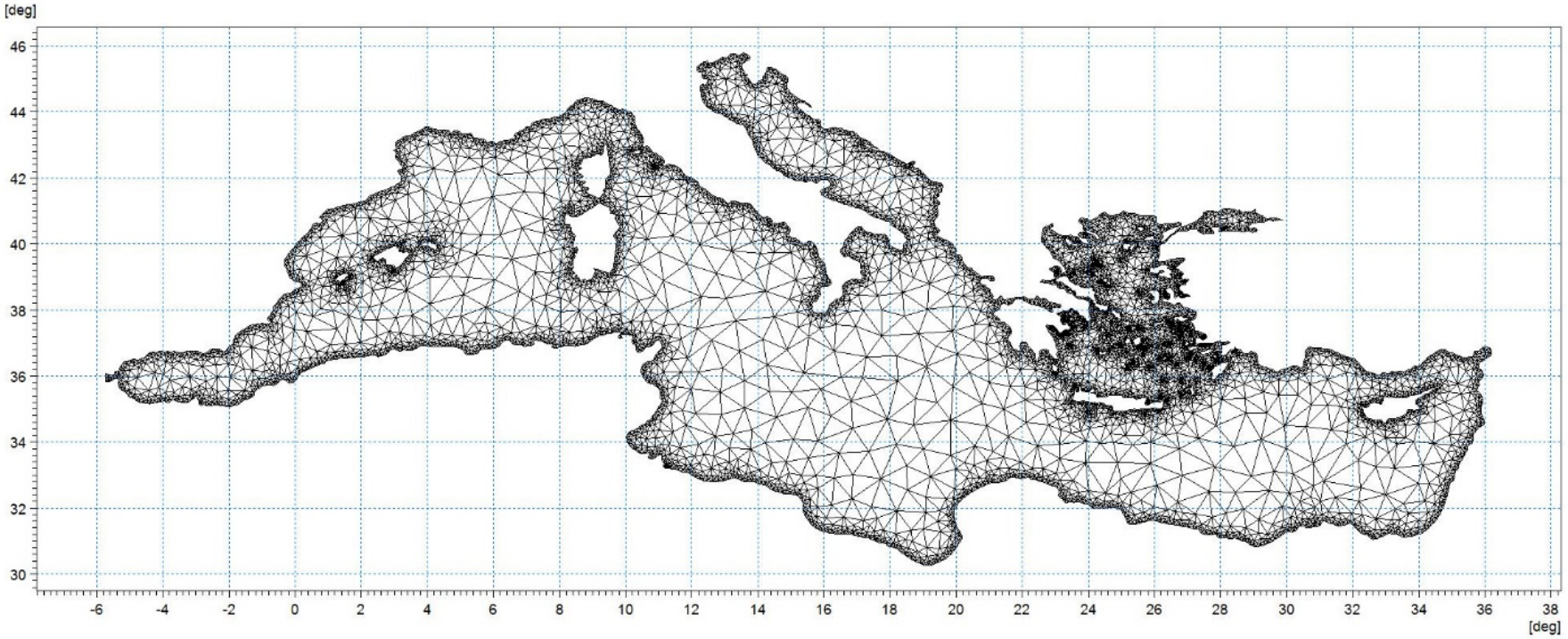

Figure 6 Mediterranean Sea computational mesh

The Pelamis is a floating device composed of 2 degrees of freedom joints connecting 3.5 m diameter steel cylinders that contain the Power Take-Off (PTO) system. The Pelamis's PTO unit is hydraulic based. Four piston assemblies in each joint resist the wave induced motion of the cylinders accommodating for vertical and horizontal motion. The pistons act as pumps for a hydraulic motor that drives an electrical generator [Drew et al., 2009, Pelamis Wave Power, 2009].

Figure 7 The Pelamis WEC (http://www.power-technology.com/projects/pelamis/)

A single Pelamis machine is a 150 m long, 700 ton device (including mooring weight) with a peak power rating of 750 kW [Pelamis Wave Power, 2009] at the manufacture and installation price of $2.4 million [Dalton et al., 2010]. WECs within a farm are commonly arranged in several rows facing the wave frontage in order to maximize their energy capture ratio [Boud, 2012]. For this study, a three-row deep Pelamis farm that can extract 20% of the incoming wave power is considered.

The output of the MIKE21 SW model run was used to calculate the potential for wave energy extraction for each country in the study area. Those wave energy potentials were calculated given the average wave power on each country's shorelines.

3. Financial accounts analysis

Average Levelized Costs of Energy (LCOE) in 2010 dollars for each electrical energy production technology were compiled from several sources to enable economic assessment of the different scenarios (Table 3). The cost of producing electricity for each scenario is obtained through a multiplication of the forecasted electricity production of each source in megawatt-hour with its LCOE.

Table 3 Levelized cost of electricity generation per energy source in USD/MWh in 2010 dollars

LCOE (USD/MWh)		Reference
Oil	104.63	[Sicilia and Keppler, 2010]
Solar	149.75	[Lazard, 2014][a]
Hydro	144.5	[El Fadel et al., 2013]
Nat.gas	155.5	[Lazard, 2014][a]
Wind	54.5	[Lazard, 2014][a]
Coal	111	[Lazard, 2014][a]
Wave	464.27	[Salvatore, 2013][b]

[a] Reflects production tax credit, investment tax credit and accelerated asset depreciation, as applicable. Assumes 2010 dollars, 20-40-year economic life, 40% tax rate and 5-40 year tax life. Assumes 30% debt at 8.0% interest rate, 50% tax equity at 8.5% cost and 20% common equity at 12% cost for Alternative Energy generation technologies. Assumes 60% debt at 8.0% interest rate and 40% equity at 12% cost for conventional generation technologies. Assumes coal price of $2.50 per MMBtu and natural gas price of $5.50 per MMBtu.

[b] Adjusted from 2013 dollars to 2010 dollars using a cumulative inflation rate of -6.4%

Positive environmental externalities were estimated based on the 2010 carbon market price range of mitigated GHGs of 15.7 to 19.17 USD/tCO2e [Ecosystem Marketplace, 2011].

CHAPTER III
RESULTS AND DISCUSSION

D. Wave resource

In this section, the validation of the Ayat [2013] study and the wave simulation output is discussed.

1. Validatio

The result of the model validation run of MIKE21 SW is shown side by side with the results of the Ayat [2013] study in Figure 9 with left side of Figure 9 representing the results of the Ayat 2013 study acquired directly from the published document. The two results show good match with slight differences due to the fact that the Ayat, 2013 study used a lower resolution mesh of 4098 nodes and 7035 elements whereas this study used a mesh with 8139 nodes and 13651 elements. As per the Ayat, 2013 study, the most energetic coastal regions occur along the southern model boundary falling between latitudes 26^{o} and 30^{o} with an average wave power of 4.5 kW/m.

2. Simulation Output

To cover the entire Mediterranean sea, another MIKE21 SW model run was performed with the same model parameters as the validated model, with a larger mesh (Figure 6). Simulation results revealed large spatial variability and are depicted in Figure 9 which shows that wave power increases with distance from shore. This finding is

congruent with wave power's positive correlation with wind fetch distance known for possessing the most energetic locations.

To demonstrate the nearshore spatial variability within the study area, Figure 10 shows the variation of wave power of a line fixed at 500 m offshore. This line traces the Mediterranean frontage in counter-clockwise order. The average wave power along the 7, 848 Km frontage line is about 2.53 KW/m with the most energetic part lying in the Egyptian regional waters. Considering the Pelamis wave farm arranged as described in the methodology, this would amount to an average extraction along the frontage of around 506 W/m.

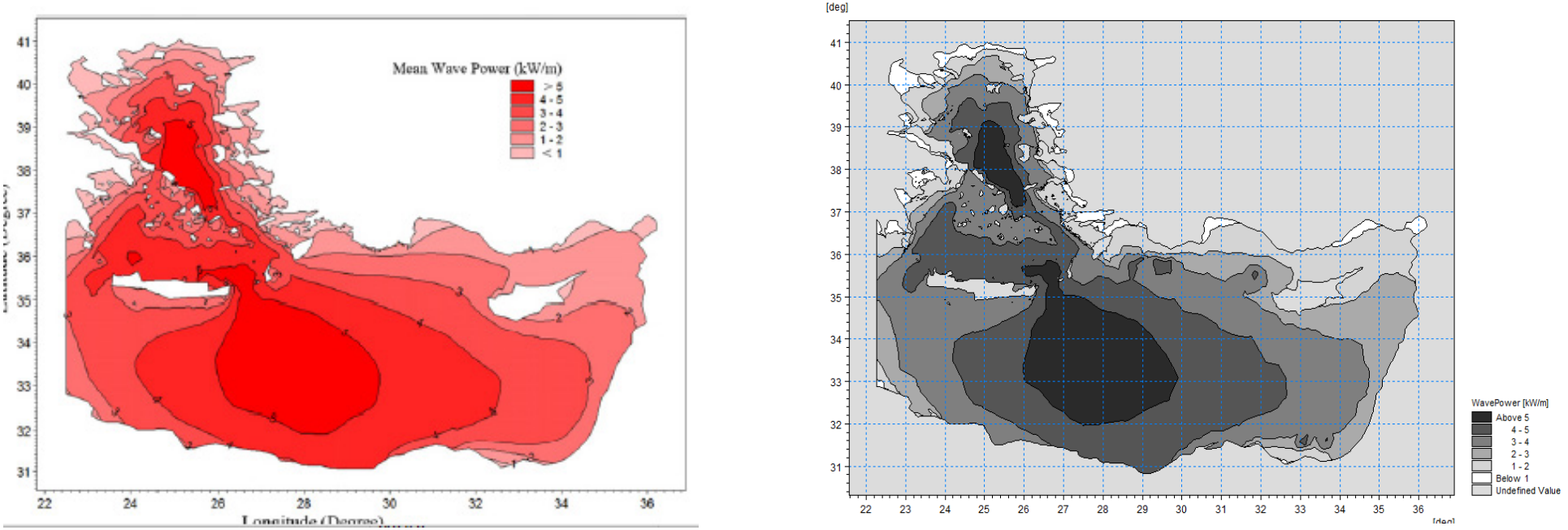

Figure 8 Ayat 2013 study results (left), MIKE21 SW model results (right)

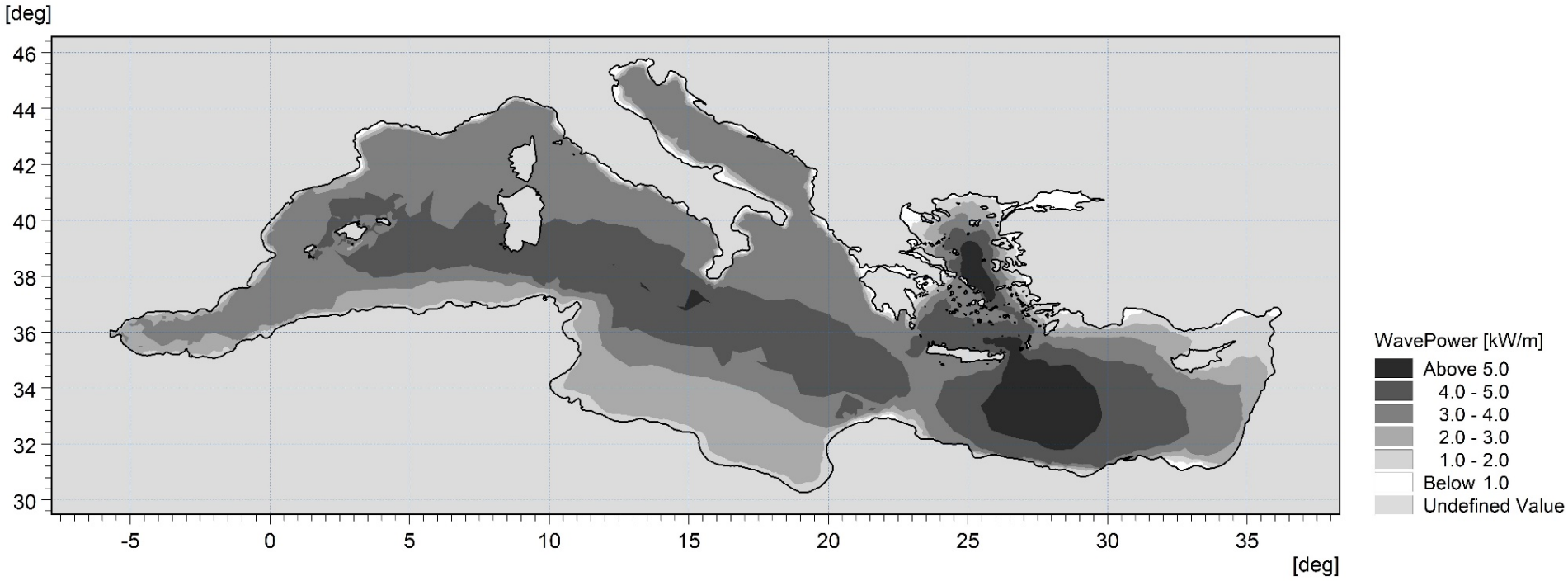

gure 9 Mean wave power (in KW/m) for the 15 year dataset

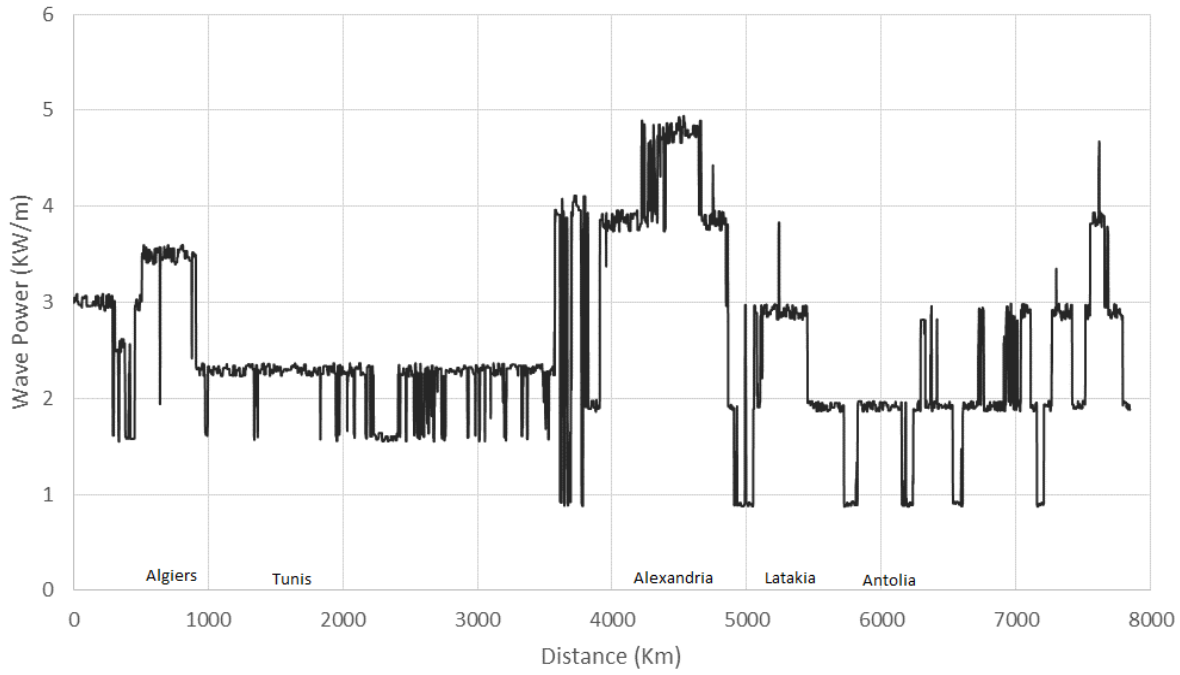

Figure 2 Variation of wave power over frontage line

The output of MIKE21 SW which provided the wave energy potential of each country in the study area was utilized for the *RevolutionW* scenario which adds the wave component to the *Revolution* scenario.

E. RE Penetration

LEAP simulations revealed significant heterogeneity in GHG emissions for countries in the study area under the *Policy* and *Revolution*/*RevolutionW* scenarios. This is due to the country-specific energy mixes (typically controlled by current technologies and available supplies) and demand parameters. For example, Turkey, with the highest demand and a significant reliance on coal for its energy supply, emerges as the highest emitter of GHGs in the study area followed by Egypt and Algeria.

The total GHG emissions from the energy sector in million tons of carbon dioxide equivalents (CO2e) are shown in Figure 11 for each of the countries in the study area. Those figures represent total GHG emissions for the entire simulated period (2000 to 2040) under the simulated scenarios. Furthermore, Figures 12 and 13 show the percent reduction in GHG emissions and the GHG savings of each scenario as compared to the baseline scenario.

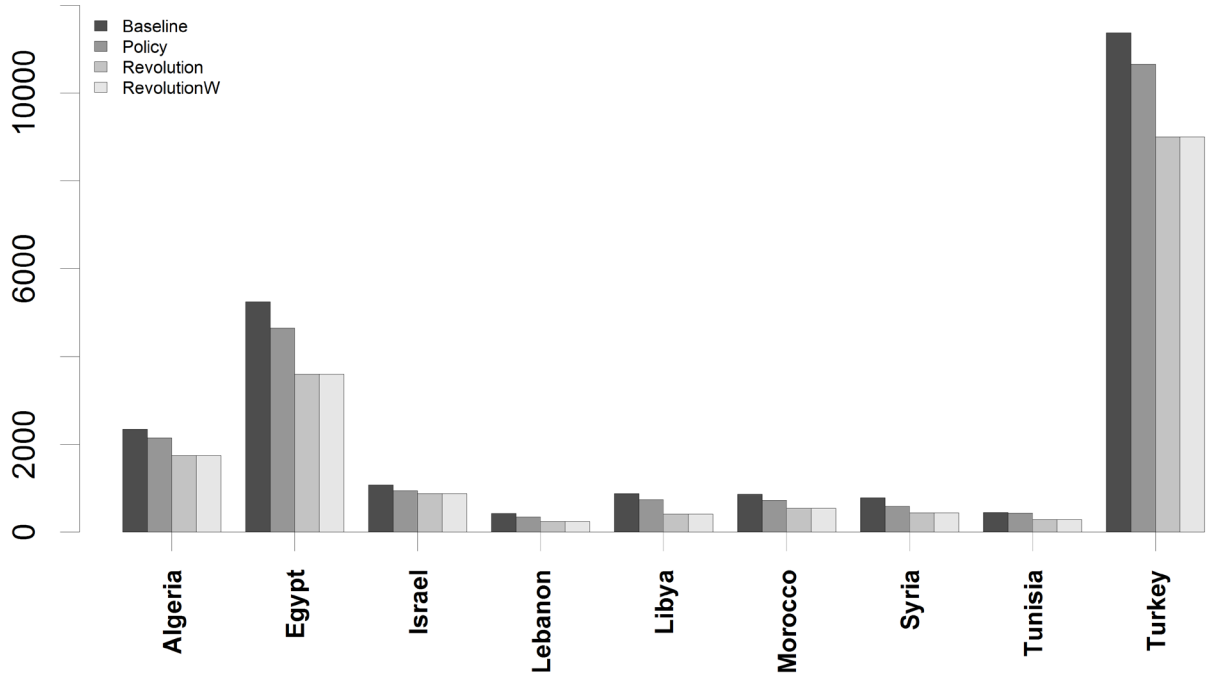

Figure 11 Energy sector GHG emissions in million tons of carbon dioxide equivalents (MtCO2e) for each scenario

In comparison to the *Baseline* scenario, the percent reductions in GHG emissions estimated under the *Policy* scenario ranged from as low as 3.26 % in Tunisia (155 MtCO2e) to as high as 24.85% in Syria (344 MtCO2e). GHG emissions on a country-by-country basis under the *Policy* scenario as forecasted for the study period, ranged from as low as 431 MtCO2e in Lebanon to as high as 11365 MtCO2e in Turkey. The reduction in country level GHG emissions ranged from as low as 14.6 MtCO2e in Tunisia (a reduction of 3.26%) to as high as 714 MtCO2e in Turkey (6.28%).

Under the *Revolution* and *RevolutionW* scenarios, national GHG emissions ranged from as low as 247 MtCO2e in Lebanon to as high as 9000 MtCO2e in Turkey whereas the corresponding GHG emissions reduction at the national level ranged from as low as 155 MtCO2e (35%) in Tunisia to as high as 2364 MtCO2e (21%) in Turkey.

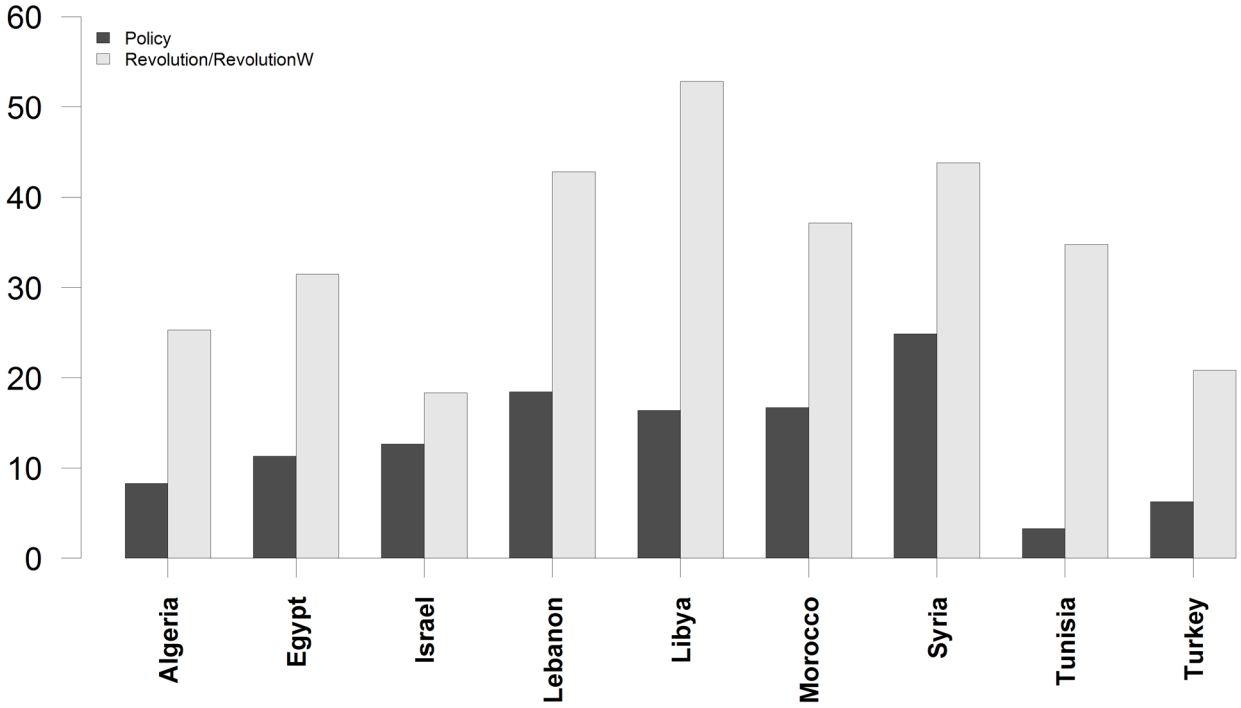

Figure 3 Percent reduction in GHG emissions for the mitigation scenarios

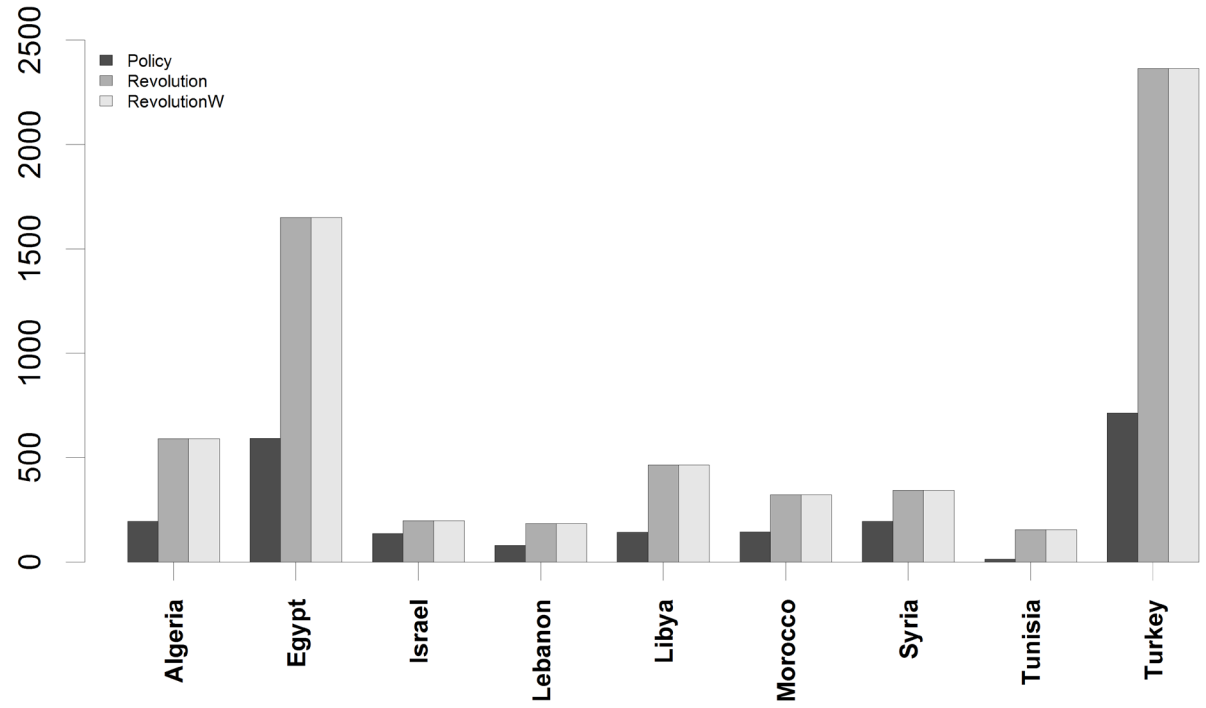

Figure 13 GHG savings in MtCO2e of each scenario wrt baseline scenario

As expected, it is apparent that the heterogeneous combinations of energy sources in the study area as well as local energy demand peculiarities have played the critical roles in defining emissions reductions in individual countries.

F. Economic implication

RE penetration in the study area's energy mix is associated with GHG emission reductions but is likely to be constrained by a relatively high initial investment. Figure 14 summarizes the estimated electricity generation costs (reference year 2010, discount rate 5%) over the whole projection period (2000–2040) under each scenario (with the first scenario year being 2010) on a country-by-country basis.

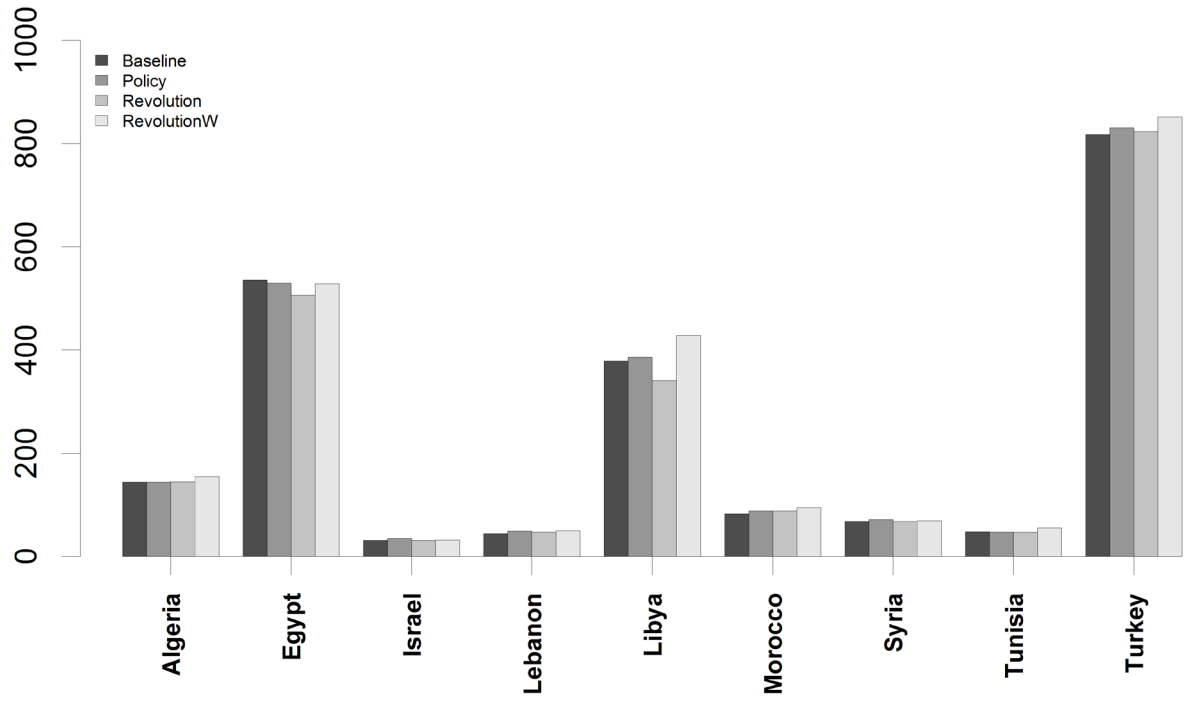

Figure 14 Estimated electricity generation costs in billions of USD (reference year 2010, discount rate 5%)

The total cost of electricity production is different among the study area countries and under the different scenarios. Figure 15 illustrates the change in investment for the *Policy*, *Revolution* and *RevolutionW* RE deployment scenarios compared to the *Baseline* scenario over the simulation period. The negative values indicate savings in investment.

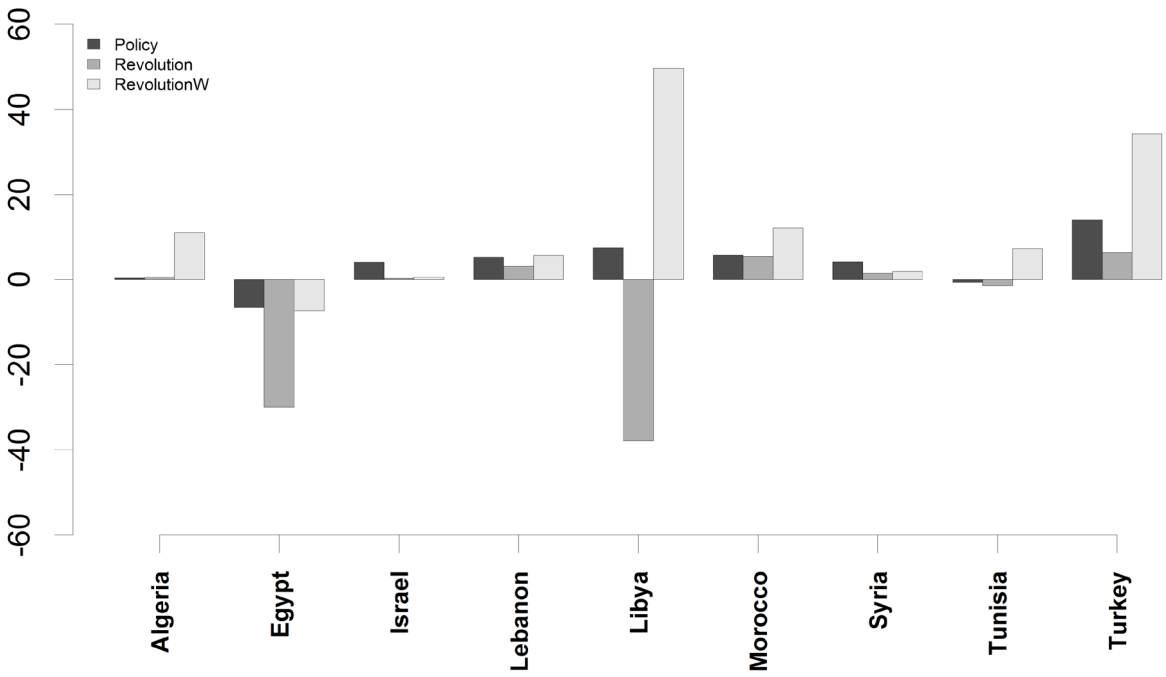

Figure 15 Percent change in investment for RE deployment scenarios with respect to the baseline scenario (Bn 2010 USD, i=0.05)

In some countries, the *Policy* and *Revolution* mitigation scenarios reveal savings on investment as compared to the *Baseline* scenario of up to 10% (Libya) for the *Revolution* scenario and 1.4% (Tunisia) for the *Policy* Scenario. Table 5 displays the percent and dollar value change in investment for each mitigation scenario with respect to the baseline scenario. For the whole study area compared to the *Baseline* scenario, the *Policy* scenario would cost an extra 34 BnUSD and has a 2217 MTCO2e potential reduction in GHG emissions over the study period. With a potential 6277 MTCO2e decrease in GHG emissions and a potential 52 BnUSD reduction in cost, the RE *Revolution* scenario emerges as an efficient scenario in the study area. While it might seem counterintuitive for the revolution scenario to be the least costly given the high initial investments in RE technologies, renewables have lower LCOE (see Table 3). The *RevolutionW* scenario offering the same GHG emissions reduction potential, entails a 115 BnUSD increase in cost.

Offsets in GHG emission entail measurable positive externalities that can be traded in global carbon markets. If these carbon credits are sold or if taxes are enforced to reach the

RE penetration scenarios goals, the revenues would be subtracted from the cost, making the RE options more attractive. Accordingly based on the carbon market price [EcosystemMarketplace, 2011], the avoided GHG emissions under the RE penetration scenarios with respect to the baseline scenario was quantified in Table 5 using the average market value of 17.45 USD/tCO2e.

Table 4 Change in investment for mitigation scenarios wrt baseline scenarios

	Policy		Revolution		RevolutionW	
Change	%	BnUSD	%	BnUSD	%	BnUSD
Algeria	0.3	0.4	0.4	0.6	7.7	11.0
Egypt	-1.2	-6.5	-5.6	-30.0	-1.4	-7.3
Israel	13.4	4.1	1.1	0.3	1.9	0.6
Lebanon	11.9	5.3	7.2	3.2	13.0	5.7
Libya	2.0	7.5	-10.0	-37.9	13.1	49.7
Morocco	7.0	5.8	6.6	5.5	14.7	12.1
Syria	6.2	4.2	2.1	1.4	2.9	2.0
Tunisia	-1.4	-0.7	-2.8	-1.4	15.1	7.3
Turkey	1.7	14.0	0.8	6.3	4.2	34.3

.

Table 1 Mitigated GHG emissions under the RE penetration scenarios

Scenario	Policy			
Parameter	Cost (BnUSD)	GHGsavings (MTCo2e)	Avg. price of avoided GHG emissions (BnUSD)	Adjusted Cost (BnUSD)
Algeria	144.37	194.69	3.4	140.97
Egypt	528.97	593.33	10.35	518.62
Israel	34.86	136.44	2.38	32.48
Lebanon	49.32	79.62	1.39	47.93
Libya	386.12	143.91	2.51	383.61
Morocco	88.36	145.48	2.54	85.82
Syria	71.53	195.45	3.41	68.12
Tunisia	47.44	14.6	0.25	47.19
Turkey	830.67	714.03	12.46	818.21
Study area	**2181.64**	**2217.55**	**38.7**	**2142.94**

Scenario	Revolution			
Parameter	Cost (BnUSD)	GHGsavings (MTCo2e)	Avg. price of avoided GHG emissions (BnUSD)	Adjusted Cost (BnUSD)
Algeria	144.53	592.39	10.34	134.19
Egypt	505.53	1650.5	28.8	476.73
Israel	31.08	197.76	3.45	27.63
Lebanon	47.24	184.72	3.22	44.02
Libya	340.76	465.11	8.12	332.64
Morocco	88.04	322.66	5.63	82.41
Syria	68.79	344.66	6.01	62.78
Tunisia	46.75	155.37	2.71	44.04
Turkey	822.97	2364.3	41.26	781.71
Study area	**2095.69**	**6277.47**	**109.54**	**1986.15**

Scenario	RevolutionW			
Parameter	Cost (BnUSD)	GHGsavings (MTCo2e)	Avg. price of avoided GHG emissions (BnUSD)	Adjusted Cost (BnUSD)
Algeria	154.99	592.39	10.34	144.65
Egypt	528.17	1650.5	28.8	499.37
Israel	31.32	197.76	3.45	27.87
Lebanon	49.78	184.72	3.22	46.56
Libya	428.33	465.11	8.12	420.21
Morocco	94.7	322.66	5.63	89.07
Syria	69.3	344.66	6.01	63.29
Tunisia	55.37	155.37	2.71	52.66
Turkey	850.91	2364.3	41.26	809.65
Study area	**2262.87**	**6277.47**	**109.54**	**2153.33**

CHAPTER IV
CONCLUSION

In this study it was found that the increased RE penetration in power generation in the study area is justifiable by the multitude of social benefits associated with RE including GHG emissions reductions, green jobs, sustainable energy, and energy security. While the initial investment in RE is relatively high, it is expected to decline with technology advances and economies of scale which will further facilitate and catalyze the shift to RE at the local and global levels. Wave energy extraction in particular was found to be so costly so that its inclusion in an RE penetration energy mix scenario would make it economically prohibitive. This high cost is not only due to the developing nature of the technology, but also to the relatively low power density of the Mediterranean Sea.

APPENDIX I.

BRIEF OVERVIEW OF SPECTRAL WAVE THEORY

MIKE 21 spectral wave module, the model used to simulate the wave parameters in this study is based on the spectral wave theory. Spectral wave theory's origins are in "description of noise" by Tukey and Hamming in their book "Measuring noise color 1" published in 1948 [Brillinger, 2002] and first applied to ocean waves by Barber and Ursell in 1948 and Deacon in 1949. The most basic form of a spectral formulation of the sea surface is called a random phase/amplitude model.

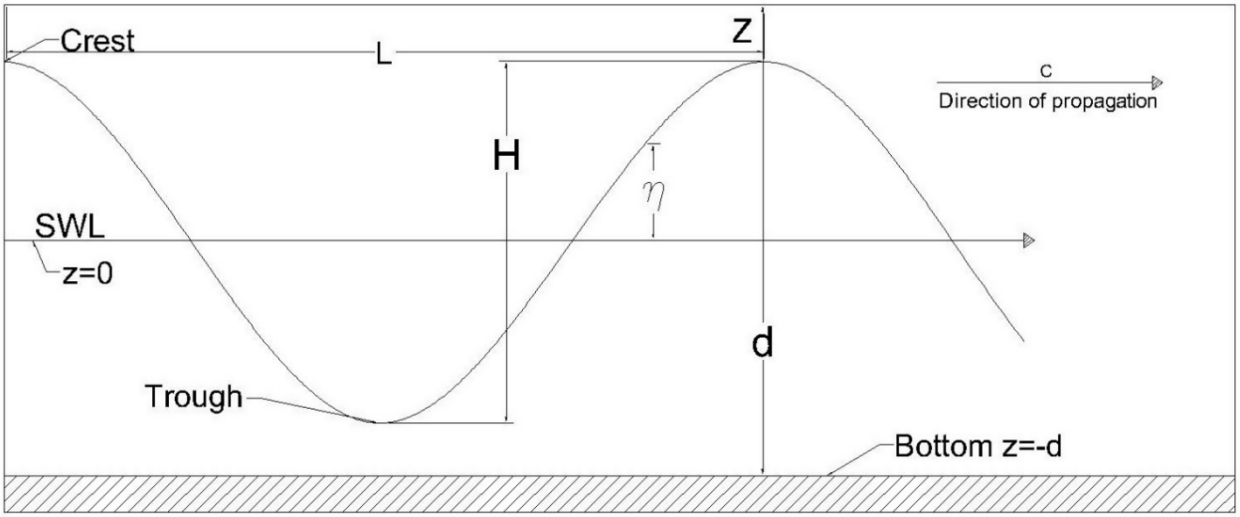

Figure 1 Simple periodic wave

As a reference, Figure 1 summarizes the basic parameters used in the following description of a random phase/amplitude model. Such a model treats the sea surface elevation $\eta(t)$ of a wave record of duration D as a Fourier series of harmonic components. This record is assumed to be the realization of a random (stochastic) process [USArmyCorpsOfEngineers, 2002]. The sea surface elevation as formulated by a random phase/amplitude model is detailed in Equation 1.

$$\eta(x,y,t) = \Sigma_{i=1}^{N}\Sigma_{j=1}^{N} a_{ij}\cos(2\pi f_i t - k_i x\cos(\theta_j) - k_j \mathrm{y}\cos(\theta_j) + \alpha_{ij} \quad (1)$$

where $i(0 \rightarrow N)$ indexes the frequency f of the wave, and $j(0 \rightarrow M)$ indexes the wave direction θ. a_{ij} and α_{ij} are the amplitude (part of the wave height H above the still water level *SWL*) and phase corresponding to frequency $f_i = i/D$ and direction $\theta_j = 2\pi j/D$. The wave number k is $2\pi/L$ with L being the wave length. Fourier analysis of this series yields a discrete amplitude spectrum and a phase spectrum. Phase spectral values show no preference between 0 and 2π and the amplitude spectrum alone characterizes the wave profile.

In a random phase/amplitude model, the variance of the average amplitude $\frac{1}{2}a^2$, and not the amplitude itself, is used to create the spectrum. This is due to the direct relation between wave power and this variance (as such variance density spectra are also called energy spectra). This spectrum is discontinuous having frequency bins of $\Delta f = f_i - f_{i-1} = 1/D$ and directional bins $\Delta\theta = \theta_j - \theta_{j-1} = 2\pi/D$. A continuous spectrum is obtained by evaluating the spectrum as $\Delta f \rightarrow 0$ and $\Delta\theta \rightarrow 0$. The variance of the average amplitude is replaced by its expected value $E\left\{\frac{1}{2}a^2\right\}$ in congruence with the assumption of it being a realization of a stochastic process. This yields a continuous variance density spectrum defined in Equation 2 [USArmyCorpsOfEngineers, 2002].

$$E(f,\theta) = \lim_{\Delta f\rightarrow 0}\lim_{\Delta\theta\rightarrow 0}\frac{1}{\Delta f\Delta\theta}E\left\{\frac{1}{2}a^2\right\} \quad (2)$$

Wave energy spectra are not used in wave models since $E(f, \theta)$ is not conserved during propagation in the presence of ambient current [Longuet-Higgins and Stewart, 1960]. Wave action, however, is conserved in the presence of currents. Action density $N(\sigma, \theta)$ (Equation 2 in the main text, section II.A.1) is used instead of energy density for most wave models including MIKE21 SW [DHI, 2012].

APPENDIX II.

ANALYTICAL APPROXIMATION TO WAVE POWER

The total energy of a wave is the sum of its kinetic energy (E_k) and its potential energy (E_p) and is defined per unit length of wave crest. Kinetic energy originates from water particle velocities due to wave motion. The kinetic energy term is defined in Equation 1 below.

$$\overline{E_k} = \int_x^{x+L} \int_{-d}^{\eta} \rho \frac{(u^2 + w^2)}{2} dz dx \tag{1}$$

Where ρ is the water density, *u* and *w* are wave velocity components in the horizontal and vertical direction and *x* and *z* are the horizontal and vertical axes respectively. Upon integration, Equation 1 yields

$$\overline{E_k} = \frac{1}{16} \rho g H^2 L \tag{2}$$

Where H is the wave height from trough to crest. On the other hand, potential energy originates from the mass of water above the wave trough. Equation 3 defines the potential energy of one wave per unit length of wave crest.

$$\overline{E_p} = \int_x^{x+l} \rho g \left\{ \frac{(\eta + d)^2}{2} + \frac{d^2}{2} \right\} dx \tag{3}$$

Where η is the sea surface elevation and *d* is the water depth. Integrating Equation 3 yields

$$\overline{E_p} = \frac{1}{6} \rho g H^2 L \tag{4}$$

Thus the total wave energy in joules per linear meter for one wavelength per unit crest width is given by Equation 5.

$$E = \frac{1}{16}\rho g H^2 L + \frac{1}{16}\rho g H^2 L = \frac{\rho g H^2 L}{8} \tag{5}$$

The total average wave energy per unit surface area (joules per square meter) is shown in Equation 6.

$$\overline{E} = \frac{E}{L} = \frac{\rho g H^2}{8} \tag{6}$$

The term wave power refers to the wave energy flux. Wave energy flux is the rate at which energy is transmitted across a vertical plan perpendicular to the wave direction of propagation and extending to the entire depth. Average wave energy flux per unit wave crest is given in Equation 7.

$$\overline{P} = \frac{1}{T}\int_{t}^{t+r}\int_{-d}^{\eta} \rho u \, dz \, dt \tag{7}$$

With *T* being the wave period. Integrating Equation 8 yields

$$\overline{P} = \overline{E} n C = \overline{E} C_g \tag{8}$$

Where $C = L/T$ is wave celerity and the wave number n is defined in Equation 9. $C_g = nC$ is the group velocity.

$$n = \frac{1}{2}\left[1 + \frac{(\frac{4\pi d}{L})}{\sinh\left(\frac{4\pi d}{L}\right)}\right] \tag{9}$$

Thus average wave power per unit wave crest is defined by Equation 10.

$$\overline{P} = \frac{1}{4}\frac{L}{T}\left[1 + \frac{(\frac{4\pi d}{L})}{\sinh\left(\frac{4\pi d}{L}\right)}\right]\rho g H^2 \tag{10}$$

APPENDIX III.

MIKE21SW DATA PROCESSING AND MODEL SETUP

G. Mesh Generation

In order to generate a flexible mesh for any Mike product, coastline and bathymetry data are required. The coastline is used to provide the model domain land boundary, and the bathymetry to provide the model domain bottom boundary. MIKE has a proprietary Mesh Generator (.mdf) application in MikeZero.

1. Coastline data

The coastline data has to be supplied to Mesh Generator in a text file formatted in the following way:

X, Y, Z, Connectivity

where:

- X is the easting/longitude value of the location on the coastline
- Y is the northing/latitude value of the location on the coastline
- Z is optional and represents the depth at the coastline.
- Connectivity is either a 1, meaning the next point is located on the same part of the coastline as the present one or 0 meaning this point represents the end of a section of coastline.

Coastline data was acquired from the Global Self-consistent, Heirarchical, High-resolution Shoreline (GSHHS) dataset available from http://www.ngdc.noaa.gov/mgg/shorelines/gshhs.html free of cost. The GEODAS software developed by NOAA was used to extract the data to *ASCII Space Delimited XYZ* format (http://www.ngdc.noaa.gov/mgg/gdas/gx_announce.Html). This file was processed using a

python script to change it from space delimited to comma separated and add a connectivity value in order to make it compatible with the requirements of the Mesh Generator. The connectivity was obtained by computing the distance between each two consecutive points and was defined as 0 if the distance is greater than the typical distance by a factor of 10 and as 1 otherwise. The scripts appends the connectivity to the end of each line in the *ASCII* file.

2. Bathymetry data

The GEBCO_08 dataset (General Bathymetric Chart of the Oceans) was used for the bathymetry. The European Marine Observation and Data Network (EMODnet) Bathymetry portal was used to access the GEBCO_08 dataset in *.asc* format.

The Mesh Generator reads bathymetry data from a proprietary MIKE file format named *dfs2*. The MikeZero Toolbox provides a tool that can be used to convert *ASCII (.asc)* formatted bathymetry to *dfs2* (MZToolbox > GIS > Grd2Mike).

H. Forcing data

Offshore wind data was obtained from the European Centre for Medium-range Weather Forecasting (ECMWF) ERA interim dataset in *.grib* binary format. GRIB (GRIdded Binary or General Regularly-distributed Information in Binary form) files are self-contained records of 2D data commonly used in meteorology. MIKE21SW requires the forcing data to be in the proprietary *.dfs2* format. The conversion process was performed by creating an "*ASCII* precursor" that the MIKEzero grid generator can parse into *.dfs2* format. The precursor was created from the *.grib* file obtained from the ECMWF using a combination of scripts in different programming languages (UNIX shell, CDO and Python) that together connect to the ECMWF MARS data server to download the *.grib* data files, dump the

contents of these files into *ASCII* files and parse these files into a *.dfs2* precursor file. In what follows is a documentation of the aforementioned scripts and the logic behind them.

1. DFS2 precursor format

Before going into a detailed documentation of the scripts, a description of the required output is requisite. An *ASCII* file that the MIKEzero grid generator can parse into *.dfs2* format is composed of two sections: the header and the body. Figure 1 shows a snippet of such a file. The first part is the header containing descriptions of the data contained in the body and the second part is part of the data contained in the first time step of u10 (zonal component of wind velocity at 10 meter altitude from the still water level).

```
"Title" "wind"
"Dim" 2
"Geo" "LONG/LAT" 21 30 0
"Time" "EqudistantTimeAxis"  "1994-01-01" "00:00:00" 40 21600
"NoGridPoints" 61 49
"Spacing" 0.1 0.1
"NoStaticItems" 0
"NoDynamicItems" 2
"Item" "u10" "v-velocity component" "m/s"
"Item" "v10" "u-velocity component" "m/s"
NoCustomBlocks 1
"M21    Misc" 1 7 0 -1E-030 -900 10 -1E-030 -1E-030 -1E-030
"Delete" -1E-030
"DataType" 0


"tstep" 1 "item" 1 "layer" 0
-2.08898_-2.14757_-2.20665_-2.11535_-1.92443_-1.73302_-1.5421_-1.62267_-1.70372_-1.78429_-
1.74572_-1.52794_-1.30968_-1.09191_-0.934193_-0.791615_-0.648548_-0.528919_-0.500111_-
0.471302_-0.442982_-0.482044_-0.566517_-0.65099_-0.734974_-0.86681_-1.02306_-1.21056_-
2.40001_-2.9049_-3.23302_-3.46349_-3.4132_-3.30236_-3.19152_-3.08995_-3.02697_-2.96447_-
2.90148_-2.85216_-2.81212_-2.77208_-2.73204_-2.80675_-2.91173_-3.06993_-3.18712_-3.12853_-
2.14025_-1.94396_-1.56212_-1.13341_-0.705189_-0.372669_-0.422474_-0.47179_-0.521595_-
0.562611_-0.38097_-0.260853_-0.174915
-2.12511_-2.30187_-2.4796_-2.40099_-2.14952_-1.89904_-1.64952_-1.81408_-1.97863_-2.14122_-
2.10509_-1.77208_-1.43908_-1.1046_-0.845325_-0.605091_-0.365833_-0.174427_-0.169056_-
0.163685_-0.157825_-0.211536_-0.30431_-0.39806_-0.491322_-0.696888_-0.902454_-1.10997_-
2.2047_-3.15734_-3.5338_-3.73449_-3.66857_-3.54943_-3.4298_-3.30724_-3.17247_-3.0382_-
2.90392_-2.82042_-2.77062_-2.7213_-2.67199_-2.66076_-2.64025_-2.5924_-2.42638_-2.21056_-
1.99376_-1.77648_-1.38976_-0.960072_-0.530872_-0.205189_-0.295521_-0.385853_-0.476673_-
0.430775_-0.381458_-0.360462_-0.348743
```

Figure 1 DFS2 ASCII precursor file snippet

The data in the body part are arranged in time steps (tstep) and items (item) in the order ["tstep" 1 "item" 1], ["tstep" 1 "item" 2], ["tstep" 2 "item" 1] etc... Each line under a particular tstep-item combination corresponds to the data points belonging to the same latitude level separated by an underscore [_] that belong to that particular combination.

2. Script structure

The scripts were written under a Linux environment and the directory structure is as illustrated in Figure 2 with the filenames enclosed in "|…|" representing different output files.

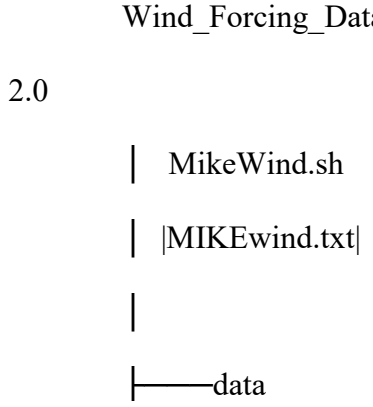

Figure 24 Scripts directory tree

The shell script "MikeWind.sh" quoted in Code 1 controls the sequence of execution of other scripts and calls Climate Data Operators (CDO). The script asks the user whether or not to download new wind data from the ECMWF MARS data server. If the user requires new data downloaded, the script will ask for the parameters that the user requires and store those parameter in the "parms.dat" file under the "order" directory and call the "MARSrequestBuilder.py" under the "source" directory that will build the "MARSrequest.py" file (given the parameters stored in the "parms.dat") under the "order" directory. The shell script then executes "MARSrequest.py" which initiates a download of the requested data placed in the "wind.grib" file under the "data" directory. Code 2 and Code 3 quote "MARSrequestBuilder.py" and "MARSrequest.py" respectively.

```
clear
echo 'download new wind data (y/n)?'
read dlq
dl="y"

if [ "$dlq" == "$dl" ]; then
        if [ -s ./order/parms.dat ]; then
                rm ./order/parms.dat
        fi
        if [ -s ./order/MARSrequest.py ]; then
                rm ./order/MARSrequest.py
        fi
        echo 'enter new grid ("NN/WW/SS/EE"in degrees)'
        read grid
        echo 'enter date range ("YYYY-MM-DD/to/YYYY-MM-DD")'
        read dat
```

Code 1 MikeWind.sh

```
top="#!/usr/bin/env python\nfrom ecmwfapi import ECMWFDataServer\nserver =
ECMWFDataServer()\nserver.retrieve({\n\t\"class\": \"ei\",\n\t\"dataset\":
\"interim\",\n\t\"grid\": \"0.25/0.25\",\n\t\"levtype\": \"sfc\",\n\t\"param\":
\"165.128/166.128\",\n\t\"step\": \"0\",\n\t\"stream\": \"oper\",\n\t\"target\":
\"wind.grib\",\n\t\"time\": \"00/06/12/18\",\n\t\"type\": \"an\",\n"
```

Code 2 MARSrequestBuilder.py

```
#!/usr/bin/env python

from ecmwfapi import ECMWFDataServer

server = ECMWFDataServer()

server.retrieve({

        "class": "ei",

        "dataset": "interim",

        "grid": "0.1/0.1",
```

Code 3 MARSrequest.py

Once this point in execution is reached (or if the user did not opt to download new data and use an existing "wind.grib" file), the shell script calls a Climat Data Operator (`cdo outputsrv wind.grib >> wind.txt`) that will dump the binary content of the "wind.grib" file into an *ASCII* file named "wind.txt", a decompression of the binary "wind.grib" file that can reach up to several Gigabytes in size. Figure 3 shows a snippet of the "wind.txt" file.

```
165      0 20140101   0     61     49 0 0
  -2.08898   -2.14757   -2.20665   -2.11535   -1.92443   -1.73302
   -1.5421   -1.62267   -1.70372   -1.78429   -1.74572   -1.52794
  -1.30968   -1.09191  -0.934193  -0.791615  -0.648548  -0.528919
 -0.500111  -0.471302  -0.442982  -0.482044  -0.566517   -0.65099
 -0.734974   -0.86681   -1.02306   -1.21056   -2.40001    -2.9049
  -3.23302   -3.46349    -3.4132   -3.30236   -3.19152   -3.08995
  -3.02697   -2.96447   -2.90148   -2.85216   -2.81212   -2.77208
  -2.73204   -2.80675   -2.91173   -3.06993   -3.18712   -3.12853
  -2.14025   -1.94396   -1.56212   -1.13341  -0.705189  -0.372669
 -0.422474   -0.47179  -0.521595  -0.562611   -0.38097  -0.260853
 -0.174915   -2.12511   -2.30187    -2.4796   -2.40099   -2.14952
  -1.89904   -1.64952   -1.81408   -1.97863   -2.14122   -2.10509
  -1.77208   -1.43908    -1.1046  -0.845325  -0.605091  -0.365833
```

Figure 3 CDO *.grib* to ASCII output snippet

This file has to be parsed into the format described under heading 1. DFS2 precursor format. A python script that does this task was written and is quoted in Code 4. This script will write the MIKEwind.txt file under the root heading. This file can be used with the MIKEzero Grid tool to generate a usable *.dfs2* file.

```
#file management
windFile="./data/wind.txt"
parms=open("./order/parms.dat").readlines()
doc0=file("MIKEwind.txt",'a')



#Write header
#lines=open(windFile).readlines()
lentsteps=0
lenlines=0
with open(windFile) as lines:
    for line in lines:
        lenlines=lenlines+1
        if (line[0:4] == " 165") or (line[0:4] == " 166"):
            lentsteps=lentsteps+1
line0=open(windFile).readline()


dfsHeadl=list()
dfsHeadl.append("\"Title\" \"wind\"\n\"Dim\" 2\n")
dfsHeadl.append("\"Geo\" \"LONG/LAT\" "+parms[0].split('/')[1]+"
"+parms[0].split('/')[2]+" 0\n\"Time\" \"EqudistantTimeAxis\"  \"1994-01-01\" \"00:00:00\"
"+str(lentsteps/2)+" 21600\n")
dfsHeadl.append("\"NoGridPoints\" "+line0.split()[4]+" "+line0.split()[5]+"\n")
dfsHeadl.append("\"Spacing\" 0.1 0.1\n\"NoStaticItems\" 0\n\"NoDynamicItems\"
2\n\"Item\" \"u10\" \"v-velocity component\" \"m/s\"\n\"Item\" \"v10\" \"u-velocity
component\" \"m/s\"\nNoCustomBlocks 1\n\"M21    Misc\" 1 7 0 -1E-030 -900 10 -1E-030 -
1E-030 -1E-030\n\"Delete\" -1E-030\n\"DataType\" 0\n")
dfsHead=dfsHeadl[0]+dfsHeadl[1]+dfsHeadl[2]+dfsHeadl[3]
```

```
tstep=[]

Tstep=[]

TstepC=[]
```

Code 4 windprocess.py

I. Model setup

In what follows is the setup file used to run the MISE21SW module, it contains all the parameters used. In order to run this setup, the script should be saved with an *.sw* extension and run in MIKE21SW.

```
// Created     : 2015-06-6 13:20:33
// DLL id      : C:\Program Files (x86)\DHI\2012\bin\pfs2004.dll
// PFS version : Feb 25 2014 19:23:51


[FemEngineSW]
  [DOMAIN]
    Touched = 1
    discretization = 2
    number_of_dimensions = 2
    number_of_meshes = 1
    file_name = |.\MEInterpolation.mesh|
    type_of_reordering = 1
    number_of_domains = 16
    coordinate_type = 'LONG/LAT'
    minimum_depth = 0
```

datum_depth = 0

vertical_mesh_type_overall = 1

number_of_layers = 10

z_sigma = -2285.199951171875

vertical_mesh_type = 1

layer_thickness = 0.1, 0.1, 0.1, 0.1, 0.1, 0.1, 0.1, 0.1, 0.1, 0.1

sigma_c = 0.1

theta = 2

b = 0

number_of_layers_zlevel = 10

vertical_mesh_type_zlevel = 1

constant_layer_thickness_zlevel = 228.5199951171875

variable_layer_thickness_zlevel = 228.5199951171875, 228.5199951171875, 228.5199951171875, 228.5199951171875, 228.5199951171875, 228.5199951171875, 228.5199951171875, 228.5199951171875, 228.5199951171875, 228.5199951171875

type_of_bathymetry_adjustment = 2

minimum_layer_thickness_zlevel = 2.285199951171875

type_of_mesh = 0

type_of_gauss = 3

[BOUNDARY_NAMES]

Touched = 0

MzSEPfsListItemCount = 1

[CODE_2]

Touched = 0

```
      name = 'Code 2'
    EndSect  // CODE_2

  EndSect  // BOUNDARY_NAMES

  [GIS_BACKGROUND]
    Touched = 0
    file_name = ||
  EndSect  // GIS_BACKGROUND

EndSect  // DOMAIN

[TIME]
  Touched = 1
  start_time = 1994, 1, 1, 0, 0, 0
  time_step_interval = 2160
  number_of_time_steps = 233720
EndSect  // TIME

[MODULE_SELECTION]
  Touched = 1
  mode_of_hydrodynamic_module = 0
  hydrodynamic_features = 1
  mode_of_spectral_wave_module = 2
```

```
  mode_of_transport_module = 0
  mode_of_mud_transport_module = 0
  mode_of_eco_lab_module = 0
  mode_of_sand_transport_module = 0
  mode_of_particle_tracking_module = 0
  mode_of_oil_spill_module = 0
EndSect  // MODULE_SELECTION

[SPECTRAL_WAVE_MODULE]
  mode = 2
  [SPACE]
    number_of_mesh_geometry = 1
  EndSect  // SPACE

  [EQUATION]
    Touched = 1
    formulation = 2
    time_formulation = 2
    JONSWAP_factor_1 = 0.92
    JONSWAP_factor_2 = 0.83
  EndSect  // EQUATION

  [TIME]
    Touched = 1
```

```
  start_time_step = 0
  time_step_factor = 1
  time_step_factor_AD = 1
EndSect  // TIME

[SPECTRAL]
  Touched = 1
  type_of_frequency_discretization = 2
  number_of_frequencies = 25
  minimum_frequency = 0.055
  frequency_interval = 0.02
  frequency_factor = 1.1
  type_of_directional_discretization = 1
  number_of_directions = 16
  minimum_direction = 0
  maximum_direction = 180
  separation_of_wind_sea_and_swell = 0
  threshold_frequency = 0.125
  maximum_threshold_frequency = 0.5959088268863615
EndSect  // SPECTRAL

[SOLUTION_TECHNIQUE]
  Touched = 1
  error_level = 0
```

```
maximum_number_of_errors = 200
minimum_period = 0.1
maximum_period = 25
initial_period = 8
scheme_of_space_discretization_geographical = 1
scheme_of_space_discretization_direction = 1
scheme_of_space_discretization_frequency = 1
method = 1
number_of_iterations = 500
tolerance1 = 1e-006
tolerance2 = 0.001
relaxation_factor = 0.1
number_of_levels_in_transport_calc = 32
number_of_steps_in_source_calc = 1
maximum_CFL_number = 1
dt_min = 0.01
dt_max = 30
type_overall = 0
file_name_overall = 'convergence_overall.dfs0'
input_format = 1
coordinate_type = ''
input_file_name = ||
number_of_points = 0
type_domain = 0
```

```
  file_name_domain = 'convergence_domain.dfsu'
  output_frequency = 5
EndSect  // SOLUTION_TECHNIQUE

[DEPTH]
  Touched = 1
  type = 0
  minimum_depth = 0.01
  format = 0
  soft_time_interval = 0
  constant_level = 0
  file_name = ||
  item_number = 1
  item_name = ''
EndSect  // DEPTH

[CURRENT]
  Touched = 1
  type = 0
  type_blocking = 1
  factor_blocking = 0.1
  format = 0
  soft_time_interval = 0
  constant_x_velocity = 0
```

```
  constant_y_velocity = 0
  file_name = ||
  item_number_for_x_velocity = 1
  item_number_for_y_velocity = 1
  item_name_for_x_velocity = ''
  item_name_for_y_velocity = ''
EndSect  // CURRENT

[WIND]
  Touched = 1
  type = 2
  format = 3
  constant_speed = 0
  constant_direction = 0
  file_name = |.\ThesisData\WaveData\Wind\MEDSEA_94-14_Wind.dfs2|
  item_number_for_x_velocity = 1
  item_number_for_y_velocity = 2
  item_name_for_x_velocity = 'u10'
  item_name_for_y_velocity = 'v10'
  soft_time_interval = 2160
  formula = 1
  type_of_drag = 1
  linear_growth_coefficient = 0.0015
  type_of_air_sea_interaction = 1
```

```
  background_Charnock_parameter = 0.01
  Charnock_parameter = 0.01
  alpha_drag = 0.00063
  beta_drag = 6.600000000000001e-005
EndSect  // WIND

[ICE]
  Touched = 1
  type = 0
  format = 3
  c_cut_off = 0.33
  file_name = ||
  item_number = 1
  item_name = ''
EndSect  // ICE

[DIFFRACTION]
  Touched = 1
  type = 0
  minimum_delta = -0.75
  maximum_delta = 3
  type_of_smoothing = 1
  smoothing_factor = 1
  number_of_smoothing_steps = 1
```

```
EndSect  // DIFFRACTION


[TRANSFER]
  Touched = 1
  type = 1
  type_triad = 0
  alpha_EB = 0.25
EndSect  // TRANSFER


[WAVE_BREAKING]
  Touched = 1
  type = 1
  type_of_gamma = 1
  alpha = 1
  gamma_steepness = 1
  type_of_effect_on_frequency = 0
  type_of_roller = 0
  roller_propagation_factor = 1
  roller_dissipation_factor = 0.15
  roller_density = 1000
  [GAMMA]
    Touched = 1
    type = 1
    format = 0
```

```
      constant_value = 0.8
      file_name = ||
      item_number = 1
      item_name = ''
      type_of_soft_start = 2
      soft_time_interval = 0
      reference_value = 0
      type_of_time_interpolation = 1
    EndSect  // GAMMA

  EndSect  // WAVE_BREAKING

  [BOTTOM_FRICTION]
    Touched = 1
    type = 3
    constant_fc = 0
    type_of_effect_on_frequency = 1
    [FRICTION_COEFFICIENT]
      Touched = 1
      type = 1
      format = 0
      constant_value = 0.0077
      file_name = ||
      item_number = 1
```

```
  item_name = ''
  type_of_soft_start = 2
  soft_time_interval = 0
  reference_value = 0
  type_of_time_interpolation = 1
EndSect  // FRICTION_COEFFICIENT

[FRICTION_FACTOR]
  Touched = 1
  type = 1
  format = 0
  constant_value = 0.0212
  file_name = ||
  item_number = 1
  item_name = ''
  type_of_soft_start = 2
  soft_time_interval = 0
  reference_value = 0
  type_of_time_interpolation = 1
EndSect  // FRICTION_FACTOR

[NIKURADSE_ROUGHNESS]
  Touched = 1
  type = 1
```

```
    format = 0
    constant_value = 0.04
    file_name = ||
    item_number = 1
    item_name = ''
    type_of_soft_start = 2
    soft_time_interval = 0
    reference_value = 0
    type_of_time_interpolation = 1
  EndSect  // NIKURADSE_ROUGHNESS

  [SAND_GRAIN_SIZE]
    Touched = 1
    type = 1
    format = 0
    constant_value = 0.00025
    file_name = ||
    item_number = 1
    item_name = ''
    type_of_soft_start = 2
    soft_time_interval = 0
    reference_value = 0
    type_of_time_interpolation = 1
  EndSect  // SAND_GRAIN_SIZE
```

```
EndSect  // BOTTOM_FRICTION

[WHITECAPPING]
  Touched = 1
  type = 1
  type_of_spectrum = 3
  mean_frequency_power = -1
  mean_wave_number_power = -1
  [dissipation_cdiss]
    Touched = 1
    type = 1
    format = 0
    constant_value = 1.5
    file_name = ||
    item_number = 1
    item_name = ''
    type_of_soft_start = 2
    soft_time_interval = 0
    reference_value = 0
    type_of_time_interpolation = 1
  EndSect  // dissipation_cdiss

  [dissipation_delta]
```

```
    Touched = 1
    type = 1
    format = 0
    constant_value = 1.5
    file_name = ||
    item_number = 1
    item_name = ''
    type_of_soft_start = 2
    soft_time_interval = 0
    reference_value = 0
    type_of_time_interpolation = 1
  EndSect  // dissipation_delta

EndSect  // WHITECAPPING

[STRUCTURES]
  type = 0
  input_format = 1
  coordinate_type = ''
  number_of_structures = 0
  input_file_name = ||
  [LINE_STRUCTURES]
    Touched = 1
    MzSEPfsListItemCount = 0
```

```
    output_of_link_data = 0
    file_name_section = 'line_section.xyz'
    number_of_structures = 0
  EndSect  // LINE_STRUCTURES

EndSect  // STRUCTURES

[INITIAL_CONDITIONS]
  Touched = 1
  type = 1
  type_additional = 1
  type_of_spectra = 1
  fetch = 100000
  max_peak_frequency = 0.4
  max_Phillips_constant = 0.0081
  shape_parameter_sigma_a = 0.07000000000000001
  shape_parameter_sigma_b = 0.09
  peakednes_parameter_gamma = 3.3
  file_name_m = ||
  item_number_m0 = 1
  item_number_m1 = 1
  item_name_m0 = ''
  item_name_m1 = ''
  file_name_A = ||
```

```
  item_number_A = 1
  item_name_A = ''
EndSect  // INITIAL_CONDITIONS

[BOUNDARY_CONDITIONS]
  Touched = 1
  MzSEPfsListItemCount = 1
  [CODE_1]
  EndSect  // CODE_1

  [CODE_2]
    Touched = 1
    type = 6
    format = 0
    constant_values = 1, 8, 270, 5, 0.1, 16, 270, 32
    file_name = ||
    item_numbers = 1, 2, 3, 4, 5, 6, 7, 8
    item_names = '', '', '', '', '', '', '', ''
    type_of_soft_start = 1
    soft_time_interval = 0
    reference_values = 0, 8, 270, 5, 0, 16, 270, 32
    type_of_time_interpolation = 1, 1, 1, 1, 1, 1, 1, 1
    type_of_space_interpolation = 1
    code_cyclic = 0
```

```
    reflection_coefficient = 1
    type_of_frequency_spectrum = 2
    type_of_frequency_normalization = 1
    sigma_a = 0.07000000000000001
    sigma_b = 0.09
    gamma = 3.3
    type_of_directional_distribution = 1
    type_of_directional_normalization = 1
    type_of_frequency_spectrum_swell = 2
    type_of_frequency_normalization_swell = 1
    sigma_a_swell = 0.07000000000000001
    sigma_b_swell = 0.09
    gamma_swell = 5
    type_of_directional_distribution_swell = 1
    type_of_directional_normalization_swell = 1
  EndSect  // CODE_2

EndSect  // BOUNDARY_CONDITIONS

[OUTPUTS]
  Touched = 1
  MzSEPfsListItemCount = 1
  number_of_outputs = 1
  [OUTPUT_1]
```

```
Touched = 1
include = 1
title = 'Output 1'
file_name = 'LB_0101_0209_AYAT_GEBCO.dfsu'
type = 1
format = 2
flood_and_dry = 2
coordinate_type = 'LONG/LAT'
zone = 0
input_file_name = ||
input_format = 1
interpolation_type = 1
first_time_step = 0
last_time_step = 1560
time_step_frequency = 1
number_of_points = 1
[POINT_1]
  name = 'Point 1'
  x = 29.23601683043659
  y = 35.91202572628406
EndSect  // POINT_1

[LINE]
  npoints = 3
```

```
    x_first = 22.26635374010095
    y_first = 30.8262972586444
    x_last = 36.20567992077223
    y_last = 40.99775419392372
  EndSect  // LINE

  [AREA]
    number_of_points = 4
    [POINT_1]
      x = 22.12696047829424
      y = 30.72458268929161
    EndSect  // POINT_1

    [POINT_2]
      x = 22.12696047829424
      y = 41.09946876327651
    EndSect  // POINT_2

    [POINT_3]
      x = 36.34507318257894
      y = 41.09946876327651
    EndSect  // POINT_3

    [POINT_4]
```

```
    x = 36.34507318257894
    y = 30.72458268929161
  EndSect  // POINT_4

EndSect  // AREA

[INTEGRAL_WAVE_PARAMETERS]
  Touched = 0
  type_of_spectrum = 1
  minimum_frequency = 0.055
  maximum_frequency = 0.5959088268863615
  separation_of_wind_sea_and_swell = 3
  threshold_frequency = 0.125
  maximum_threshold_frequency = 0.125
  hm0_minimum = 0.01
  type_of_h_max = 3
  duration = 10800
  distance_above_bed_for_particle_velocity = 0
  minimum_direction = 0
  maximum_direction = 360
  [Total_wave_parameters]
    Significant_wave_height = 1
    Maximum_wave_height = 0
    Peak_wave_period = 0
```

```
    Wave_period_t01 = 0
    Wave_period_t02 = 1
    Wave_period_tm10 = 0
    Peak_wave_direction = 0
    Mean_wave_direction = 1
    Directional_standard_deviation = 0
    Wave_velocity_components = 0
    Radiation_stresses = 0
    Particle_velocities = 0
    Wave_power = 1
  EndSect  // Total_wave_parameters

  [Wind_sea_parameters]
    Significant_wave_height = 0
    Maximum_wave_height = 0
    Peak_wave_period = 0
    Wave_period_t01 = 0
    Wave_period_t02 = 0
    Wave_period_tm10 = 0
    Peak_wave_direction = 0
    Mean_wave_direction = 0
    Directional_standard_deviation = 0
    Wave_velocity_components = 0
    Radiation_stresses = 0
```

```
    Particle_velocities = 0
    Wave_power = 0
  EndSect  // Wind_sea_parameters

  [Swell_parameters]
    Significant_wave_height = 0
    Maximum_wave_height = 0
    Peak_wave_period = 0
    Wave_period_t01 = 0
    Wave_period_t02 = 0
    Wave_period_tm10 = 0
    Peak_wave_direction = 0
    Mean_wave_direction = 0
    Directional_standard_deviation = 0
    Wave_velocity_components = 0
    Radiation_stresses = 0
    Particle_velocities = 0
    Wave_power = 0
  EndSect  // Swell_parameters

EndSect  // INTEGRAL_WAVE_PARAMETERS

[INPUT_PARAMETERS]
  Touched = 0
```

```
  Surface_elevation = 0
  Water_depth = 1
  Current_velocity_components = 0
  Wind_speed = 1
  Wind_direction = 0
  Ice_concentration = 0
EndSect  // INPUT_PARAMETERS

[MODEL_PARAMETERS]
  Touched = 0
  Wind_friction_speed = 0
  Roughness_length = 0
  Drag_coefficient = 0
  Charnock_constant = 0
  Friction_coefficient = 0
  Breaking_parameter_gamma = 0
  Courant_number = 0
  Time_step_factor = 0
  Convergence_angle = 0
  Length = 0
  Area = 0
  Threshold_period = 0
  Roller_area = 0
  Roller_dissipation = 0
```

```
      Breaking_index = 0
    EndSect  // MODEL_PARAMETERS

    [SPECTRAL_PARAMETERS]
      Touched = 0
      separation_of_wind_sea_and_swell = 3
      threshold_frequency = 0.125
      maximum_threshold_frequency = 0.125
      wave_energy = 1
      wave_action = 0
      zeroth_moment_of_wave_action = 0
      first_moment_of_wave_action = 0
      wave_energy_wind_sea = 0
      wave_energy_swell = 0
    EndSect  // SPECTRAL_PARAMETERS

  EndSect  // OUTPUT_1

 EndSect  // OUTPUTS

EndSect  // SPECTRAL_WAVE_MODULE

EndSect  // FemEngineSW
```

APPENDIX IV.

ELECTRICAL ENERGY CONSUMPTION PER CAPITA

Year	KWh/capita								
	Algeria	Egypt	Israel	Lebanon	Libya	Morocco	Syria	Tunisia	Turkey
1971	133.09	202.92	2288.69	525.58	180.24	124.89	175.47	154.18	247.08
1972	142.03	199.44	2497.14	575.15	192.92	138.53	200.77	174.90	277.26
1973	157.80	196.56	2497.56	649.89	373.58	151.72	181.56	192.25	298.18
1974	169.63	217.13	2518.21	700.85	430.72	157.27	209.94	206.78	313.25
1975	194.50	239.74	2624.89	646.43	544.68	162.70	235.59	216.54	359.42
1976	218.73	273.54	2718.09	692.74	653.76	178.18	228.95	241.02	421.51
1977	231.71	308.04	2832.00	742.45	782.64	191.77	222.80	274.55	462.67
1978	277.28	322.06	3011.92	811.94	893.70	205.29	287.68	303.00	480.51
1979	312.67	346.70	3049.39	915.63	1060.42	221.69	315.31	354.10	489.46
1980	328.32	381.47	3022.18	973.79	1129.95	235.90	355.51	402.10	496.34

1981	361.27	417.42	3067.49	1047.88	1094.75	247.71	412.95	422.41	519.80
1982	403.63	457.37	3173.90	1138.56	1064.32	261.12	519.58	410.45	543.68
1983	415.01	502.61	3313.28	1235.62	1039.30	279.33	599.15	450.53	555.42
1984	438.66	520.67	3359.46	1292.35	1020.12	281.79	588.36	467.16	613.36
1985	463.71	495.95	3485.24	1311.74	1007.13	293.28	617.12	511.13	659.16
1986	482.37	588.53	3407.07	1411.88	1057.72	305.83	605.59	530.79	697.89
1987	452.67	618.22	3756.47	1562.77	1440.80	309.71	589.81	553.95	770.14
1988	478.99	632.52	4026.11	1349.03	1546.46	339.16	627.44	586.18	808.05
1989	519.01	654.39	4228.42	840.61	1509.12	333.78	676.58	611.28	873.53
1990	528.43	674.66	4176.18	517.94	1590.57	357.11	688.51	638.43	928.44
1991	529.41	691.13	3981.21	1017.27	1674.29	369.34	700.44	651.70	964.10
1992	556.64	695.24	4568.42	1194.60	1773.62	399.71	702.40	687.41	1043.20
1993	545.02	711.70	4618.89	1366.49	1832.93	399.67	687.56	717.32	1114.14
1994	548.09	724.84	4934.25	1481.18	1846.83	418.80	751.95	766.81	1144.62
1995	557.08	744.14	5127.86	1561.61	1796.15	428.47	833.17	774.88	1226.57

1996	567.70	803.51	5340.30	2116.92	1811.33	431.07	894.26	785.98	1327.72
1997	572.91	843.94	5488.52	2507.53	1822.74	448.27	915.59	826.16	1439.46
1998	615.55	889.04	5819.46	3066.19	2114.57	476.77	960.19	868.18	1519.72
1999	649.76	947.51	5974.37	3031.05	2189.34	450.56	1015.69	947.45	1556.13
2000	680.20	984.07	6323.10	3019.43	2230.36	487.38	1068.60	992.41	1652.75
2001	705.98	1036.94	6400.22	2980.47	2261.85	522.68	1149.13	1050.71	1613.24
2002	727.72	1087.72	6502.74	3044.13	2778.55	534.54	1239.89	1079.51	1667.87
2003	783.24	1155.82	6597.31	2996.65	2953.74	581.06	1302.51	1004.19	1772.61
2004	801.04	1199.59	6525.92	2881.75	3110.00	612.73	1409.86	1043.96	1892.90
2005	887.46	1271.75	6572.20	2834.56	3426.16	635.93	1516.75	1091.93	2015.16
2006	859.66	1343.77	6711.23	2713.06	3779.32	690.71	1565.07	1115.63	2180.72
2007	891.81	1436.07	7003.25	2805.58	3765.67	720.80	1576.22	1159.99	2349.88
2008	945.10	1482.85	7134.00	2978.30	4354.06	741.52	1602.97	1198.77	2425.27
2009	864.65	1550.49	6607.89	3141.51	4342.79	752.48	1562.37	1284.63	2316.64
2010	1014.98	1589.88	6953.28	3478.78	4531.98	777.07	1880.11	1406.93	2492.20

2011	1121.63	1700.74	6930.00	3494.71	3807.02	818.52	1674.06	1335.51	2704.05
2012	1236.13	1700.45	7188.93	3102.42	4706.84	875.18	1221.72	1411.09	2789.66

REFERENCES

[Arinaga and Cheung, 2012] Arinaga, R. A. and Cheung, K. F. (2012). Atlas of global wave energy from 10 years of reanalysis and hindcast data. *Renewable Energy*, 39(1):49–64.

[Ayat, 2013] Ayat, B. (2013). Wave power atlas of eastern mediterranean and aegean seas. *Energy*, 54:251–262.

[Blumsack and Xu, 2011] Blumsack, S. and Xu, J. (2011). Spatial variation of emissions impacts due to renewable energy siting decisions in the western us under high-renewable penetration scenarios. *Energy policy*, 39(11):6962–6971.

[Boud, 2012] Boud, R. (2012). *UK wave energy resource*. Carbon Trust.

[Brillinger, 2002] Brillinger, D. R. (2002). John w. tukey's work on time series and spectrum analysis. *Annals of Statistics*, pages 1595–1618.

[Brooke, 2003] Brooke, J. (2003). *Wave energy conversion*. Elsevier.

[Cai et al., 2007] Cai, W., Wang, C., Wang, K., Zhang, Y., and Chen, J. (2007). Scenario analysis on co2 emissions reduction potential in china's electricity sector. *Energy Policy*, 35(12):6445–6456.

[Chedid et al., 2001] Chedid, R., Chaaban, F., and Salameh, S. (2001). *Policy* analysis of greenhouse gas emissions: the case of the lebanese electricity sector. *Energy Conversion and Management*, 42(3):373–392.

[Connolly et al., 2010a] Connolly, D., Lund, H., Mathiesen, B. V., and Leahy, M. (2010a). A review of computer tools for analysing the integration of renewable energy into various energy systems. *Applied Energy*, 87(4):1059–1082.

[Connolly et al., 2010b] Connolly, D., Lund, H., Mathiesen, B. V., and Leahy, M. (2010b). A review of computer tools for analysing the integration of renewable energy into various energy systems. *Applied Energy*, 87(4):1059–1082.

[Dalton et al., 2010] Dalton, G. J., Alcorn, R., and Lewis, T. (2010). Case study feasibility analysis of the pelamis wave energy convertor in ireland, portugal and north america. *Renewable Energy*, 35(2):443–455.

[DHI, 2012] DHI (2012). Mike 21 spectral wave module scientific documentation. *Dutch Hydraulic Institute*.

[Drew et al., 2009] Drew, B., Plummer, A., and Sahinkaya, M. N. (2009). A review of wave energy converter technology. *Proceedings of the Institution of Mechanical Engineers, Part A: Journal of Power and Energy*, 223(8):887–902.

[EcosystemMarketplace, 2011] EcosystemMarketplace (2011). Back to the future bloomberg new energy finance based on 2010 market.new york,us.

[El Fadel et al., 2013] El Fadel, M., Rachid, G., El-Samra, R., Boutros, G. B., and Hashisho, J. (2013). Emissions reduction and economic implications of renewable energy market penetration of power generation for residential consumption in the mena region. *Energy Policy*, 52:618–627.

[Føyn et al., 2011] Føyn, T. H. Y., Karlsson, K., Balyk, O., and Grohnheit, P. E. (2011). A global renewable energy system: A modelling exercise in etsap/tiam. *Applied energy*, 88(2):526–534.

[Henfridsson et al., 2007] Henfridsson, U., Neimane, V., Strand, K., Kapper, R., Bernhoff, H., Danielsson, O., Leijon, M., Sundberg, J., Thorburn, K., Ericsson, E., et al.

(2007). Wave energy potential in the baltic sea and the danish part of the north sea, with reflections on the skagerrak. *Renewable Energy*, 32(12):2069–2084.
[Hughes and Heap, 2010] Hughes, M. G. and Heap, A. D. (2010). National-scale wave energy resource assessment for australia. *Renewable Energy*, 35(8):1783–1791.
[IEA, 2014] IEA (2014). Key world energy statistics. *International Energy Agency*.
[Iglesias and Carballo, 2009] Iglesias, G. and Carballo, R. (2009). Wave energy potential along the death coast (spain). *Energy*, 34(11):1963–1975.
[Iglesias and Carballo, 2010a] Iglesias, G. and Carballo, R. (2010a). Offshore and inshore wave energy assessment: Asturias (n spain). *Energy*, 35(5):1964–1972.
[Iglesias and Carballo, 2010b] Iglesias, G. and Carballo, R. (2010b). Wave energy resource in the estaca de bares area (spain). *Renewable Energy*, 35(7):1574–1584.
[Iglesias and Carballo, 2010c] Iglesias, G. and Carballo, R. (2010c). Wave power for la isla bonita. *Energy*, 35(12):5013–5021.
[Iglesias et al., 2009] Iglesias, G., López, M., Carballo, R., Castro, A., Fraguela, J. A., and Frigaard, P. (2009). Wave energy potential in galicia (nw spain). *Renewable Energy*, 34(11):2323–2333.
[Kim et al., 2011] Kim, G., Jeong, W. M., Lee, K. S., Jun, K., and Lee, M. E. (2011). Offshore and nearshore wave energy assessment around the korean peninsula. *Energy*, 36(3):1460–1469.
[Lazard, 2014]Lazard, P. (2014). Levelized cost of energy analysis. Technical report, Tech. rep., Lazar Capital Markets Report, version 8.
[Leishman et al., 1976] Leishman, J., Scobie, G., and Britain, G. (1976). *The Development of Wave Power: A Techno-economic Study*. National Engineering Laboratory.
[Longuet-Higgins and Stewart, 1960]Longuet-Higgins, M. S. and Stewart, R. (1960). Changes in the form of short gravity waves on long waves and tidal currents. *Journal of Fluid Mechanics*, 8(04):565–583.
[McPherson and Karney, 2014a] McPherson, M. and Karney, B. (2014a). Long-term scenario alternatives and their implications: Leap model application of panama×³ s electricity sector. *Energy Policy*, 68:146–157.
[McPherson and Karney, 2014b] McPherson, M. and Karney, B. (2014b). Long-term scenario alternatives and their implications: Leap model application of panama×³ s electricity sector. *Energy Policy*, 68:146–157.
[Norris and Droniou, 2007] Norris, J. and Droniou, E. (2007). Update on emec activities, resource description, and characterisation of wave-induced velocities in a tidal flow. In *Proc. 7th European wave and tidal energy Conference, Porto, Portugal*.
[Panicker, 1976] Panicker, N. (1976). Power resource potential of ocean surface waves. In *Proceedings of the wave and salinity gradient workshop, Newark, Delaware, USA*, pages J1–J48.
[PelamisWavePower, 2009] PelamisWavePower (2009). Pelamis brochure.
[Salvatore, 2013] Salvatore, J. (2013). World energy perspective - cost of energy technologies. *World ENergy Council*.
[SEI, 2016] SEI. Long-range energy alternatives planning system. http://-www.energycommunity.org/?action=47. (Accessed on 07/11/2016).
[Shaw, 1982] Shaw, R. (1982). *Wave energy: a design challenge*. E. Horwood.
[Sicilia and Keppler, 2010] Sicilia, M. and Keppler, J. (2010). Projected costs of generating electricity. *International Energy Agency, Paris*.
[Simmons et al., 2007] Simmons, A., Uppala, S., Dee, D., and Kobayashi, S. (2007). Era-interim: New ecmwf reanalysis products from 1989 onwards. *ECMWF newsletter*, 110(110):25–35.

[Sorensen et al., 2004] Sorensen, O., Kofoed-Hansen, H., Rugbjerg, M., and Sorensen, L. (2004). A third-generation spectral wave model using an unstructured finite volume technique. In *Coastal Engineering Conference*, volume 29, page 894. World Scientific.
[Stahl, 1892] Stahl, A. (1892). The utilization of the power of ocean waves. *Trans. ASME*, 13:438.
[Tsoutsos et al., 2008] Tsoutsos, T., Papadopoulou, E., Katsiri, A., and Papadopoulos, A. M. (2008). Supporting schemes for renewable energy sources and their impact on reducing the emissions of greenhouse gases in greece. *Renewable and Sustainable Energy Reviews*, 12(7):1767–1788.
[USArmyCorpsOfEngineers, 2002] USArmyCorpsOfEngineers (2002). Coastal engineering manual. *Engineer Manual*, 1110:2–1100.
[WorldBank, 2010] WorldBank (2010). *World development indicators*.
[Zodiatis et al., 2014] Zodiatis, G., Galanis, G., Nikolaidis, A., Kalogeri, C., Hayes, D., Georgiou, G. C., Chu, P. C., and Kallos, G. (2014). Wave energy potential in the eastern mediterranean levantine basin. an integrated 10-year study. *Renewable Energy*, 69:311–323.